CHAPTER 3

Result and Discussion

In this results and discussion, we present results and analysis of measurement and observation for both Al doped ZnO (AZO) and Cu_2O thin films by Scanning Electron Microscopy (SEM), Energy dispersive X-ray Spectroscopy (EDS), Raman spectroscopy, X-ray diffraction (XRD) and Ultraviolet-Visible (UV-vis) spectroscopy. Moreover, electrical property was measured for both thin films. In addition, AZO/Cu_2O heterojunction was characterized and investigated.

3.1 AZO thin film

Both ZnO and AZO films were deposited on glass substrate by double tips sparking process under flowing argon atmosphere. The samples were annealed at 400 °C for 60 minutes. The doping ratio of Al into ZnO was studied by using a different capacitor paralleled Al doping tips.

3.1.1 SEM images and EDS analysis

The SEM surface morphology and cross-section images of un-doped and Al doped ZnO ,which had a different capacitance paralleled Al doping tips of 0.5, 1.1, 1.5, 3.1, and 4.7 nF, were observed. The elemental and chemical compositions of Al and Zn in the film were analyzed by EDS.

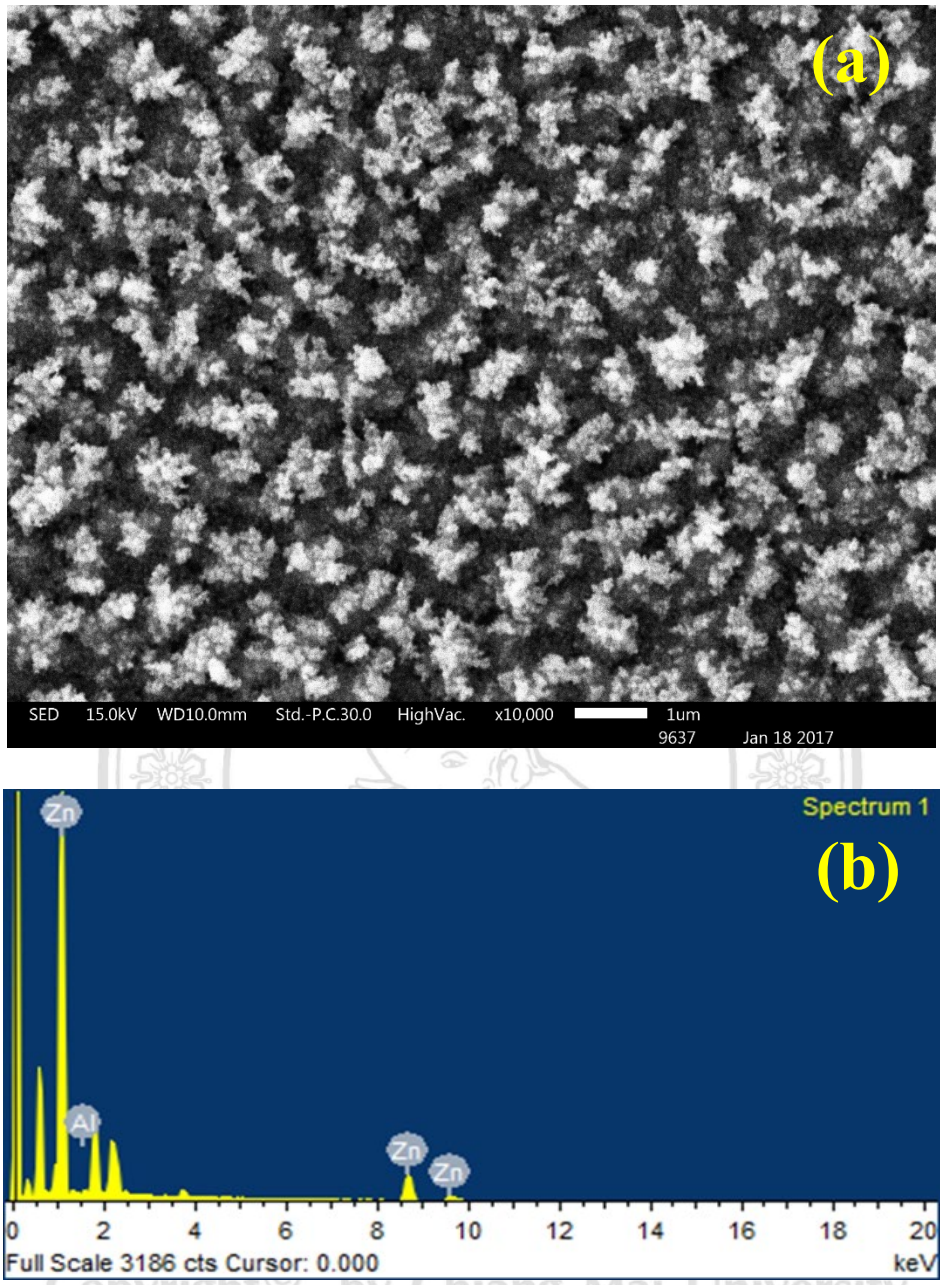

Figure 3.1 (a) Surface morphology and (b) EDS spectrum of Al doped ZnO with capacitance paralleled Al tips of 0.5 nF.

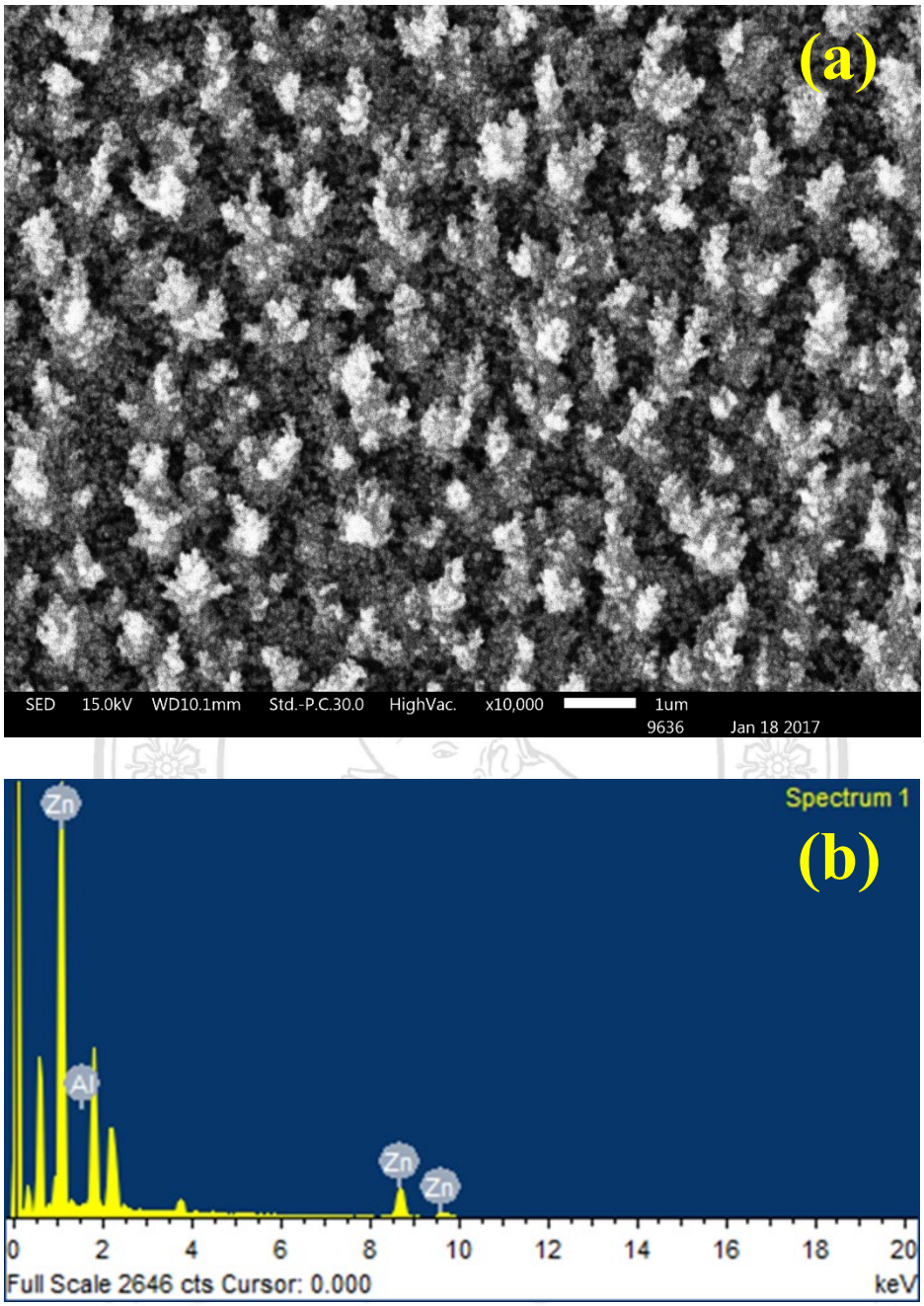

Figure 3.2 (a) Surface morphology and (b) EDS spectrum of Al doped ZnO with capacitance paralleled Al tips of 1.1 nF.

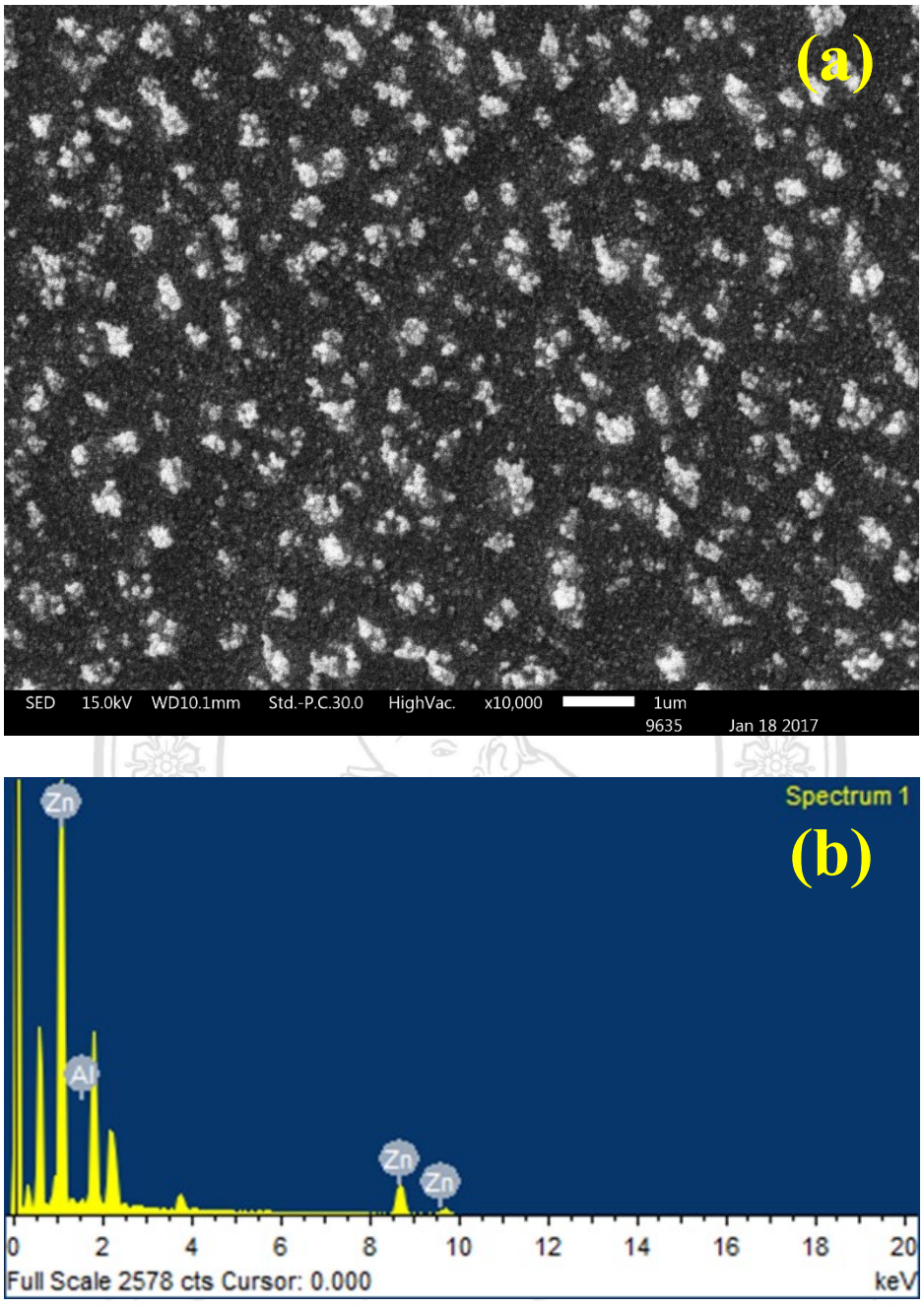

Figure 3.3 (a) Surface morphology and (b) EDS spectrum of Al doped ZnO with capacitance paralleled Al tips of 1.5 nF.

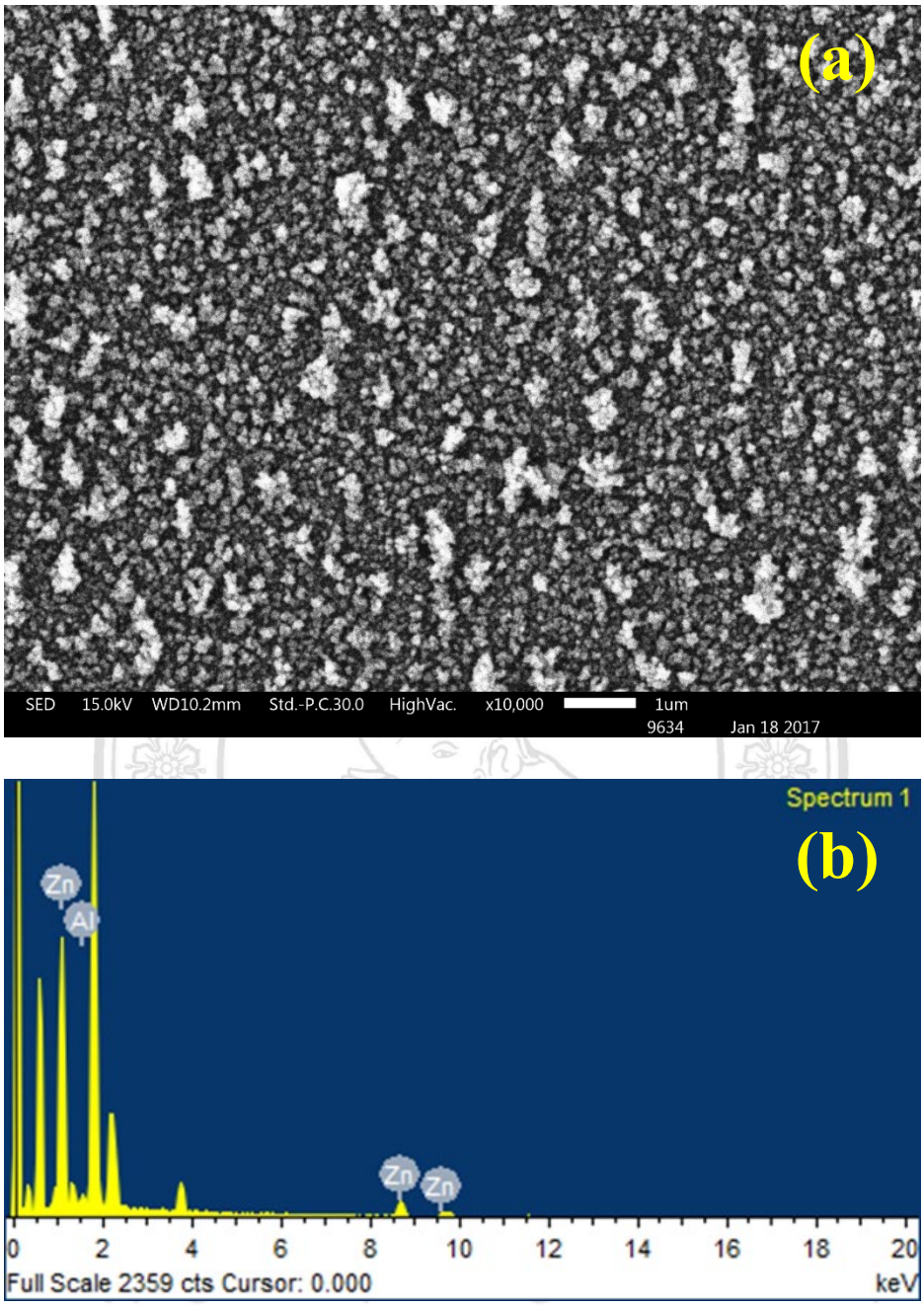

Figure 3.4 (a) Surface morphology and (b) EDS spectrum of Al doped ZnO with capacitance paralleled Al tips of 3.1 nF.

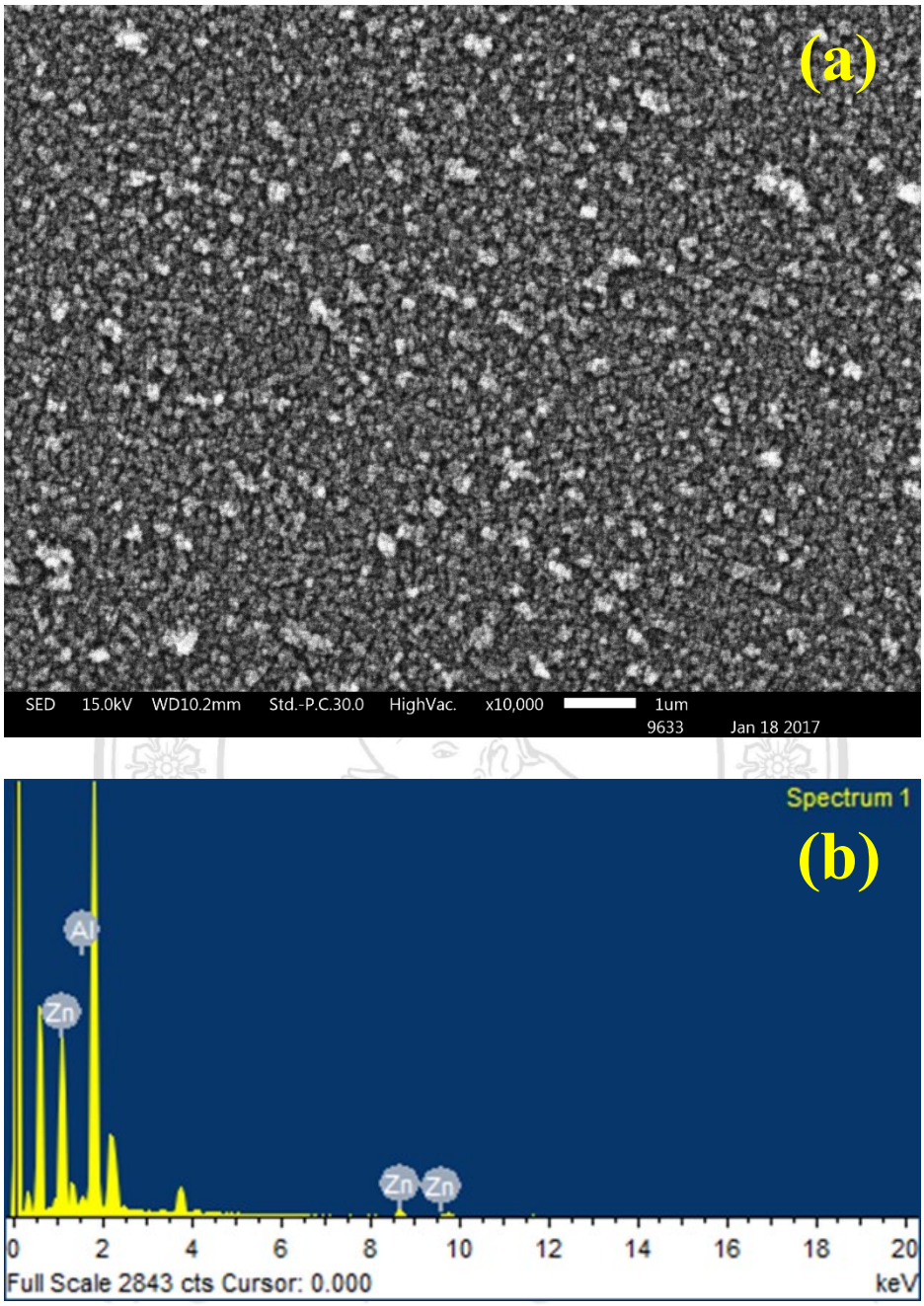

Figure 3.5 (a) Surface morphology and (b) EDS spectrum of Al doped ZnO with capacitance paralleled Al tips of 4.7 nF.

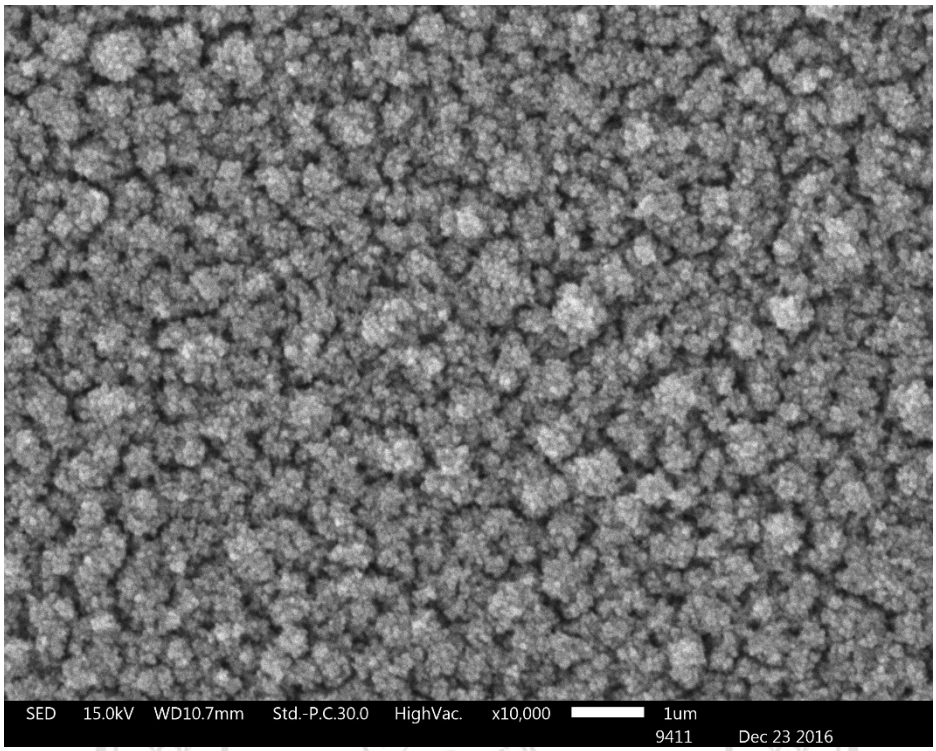

Figure 3.6 Surface morphology of un-doped ZnO.

From the surface morphology of each sample, they were used to estimate element composition of AZO films. EDS spectra of AZO samples show energy dispersive of Zn and Al. These indicated that the element in the films included Zn and Al. Moreover, intensity of Al peak is seen clearly increased when increasing the capacitance paralleled Al tips.

SEM surface morphology of un-doped and Al doped ZnO is seen clear that each sample show different surface. The film of AZO with capacitance paralleled Al tips of 0.5 nF indicated to be rather of different altitude surface. The different altitude surface characteristic decreased with AZO film which have capacitance paralleled Al tips increased. However, cross-section image of each sample represented to different altitude surface as shown in Figure 3.7.

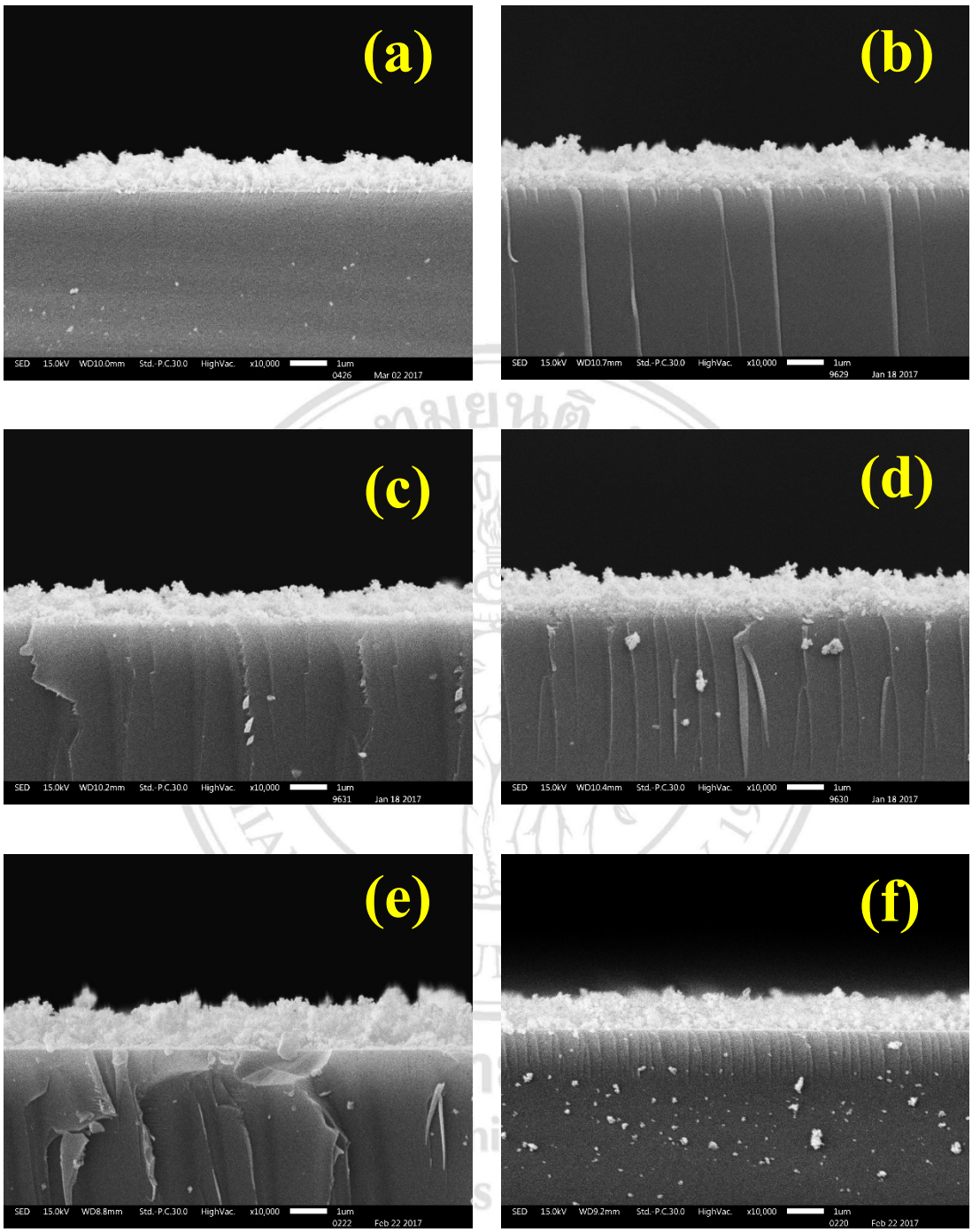

Figure 3.7 Cross-section images of (a) ZnO and AZO with capacitance paralleled Al tips of (b) 0.5, (c) 1.1, (d) 1.5, (e) 3.1, and (f) 4.7 nF.

From ESD spectrum, atomic ratio of Al in ZnO for each sample was analyzed. The thickness of all samples, prepared by sparking process for 5 minutes under flowing Ar atmosphere with flow rate of 0.5 L/min, was measured by Image J software. The atomic ratio of Al in ZnO and the film thickness were shown in Table 3.1.

Table 3.1 The Al doping ratio and the film thickness.

sample	Capacitance paralleled Zn : Al (nF)	Al doping (atomic %)	Thickness (μm)
1	40 : -	0.00 (0)	0.950
2	40 : 0.5	3.21 (3)	1.136
3	40 : 1.1	5.23 (5)	0.972
4	40 : 1.5	7.31 (7)	1.174
5	40 : 3.1	12.94 (13)	1.110
6	40 : 4.7	21.76 (22)	0.956

It is seen clearly that the Al doping ratio increased when capacitance paralleled Al tips increased and those of Zn tips was fixed at 40 nF. The thickness of the films prepared by sparking process for 5 minutes is average at 1 μm.

From Al doping ratio in ZnO increased when capacitance paralleled Al tips increased, which relates to sparking energy. It can be described in the equation as follows:

$$E = \frac{1}{2}CV^2 \tag{3.1}$$

where E is Sparking energy

C is Capacitance paralleled Al tips

V is Breakdown voltage

From equation 3.1, it shows that variation of capacitance paralleled Al tips affected directly to sparking energy at Al tips for the same breakdown voltage. When capacitance paralleled Al tips increased, Sparking energy increased. That made Al content in ZnO increased. This is a reason to explain the Al doping ratio increased when increasing capacitance paralleled Al tips.

3.1.2 Raman spectroscopy analysis

To examine the chemical structure, un-doped and Al doped ZnO thin films were examined by Raman spectroscopy. The Raman spectra were recorded in wavelength range of 200-800 nm at room temperature using the 532 nm line of solid state laser 150 mW. The Raman spectra of the samples is shown in Figure 3.8.

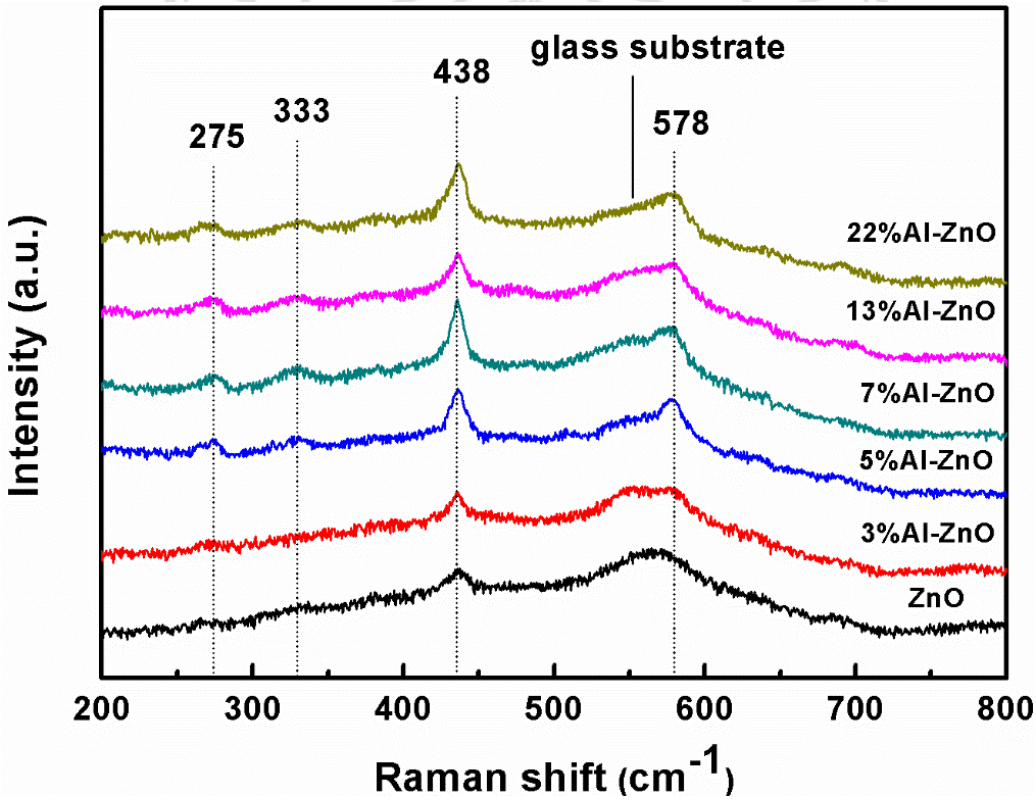

Figure 3.8 Raman spectra of un-doped and Al doped ZnO.

All samples present the Raman shift of 333 cm^{-1} (multiphonon mode) and 438 cm^{-1} (E_2 high mode) [25], which associated with O sublattice vibrations of a typical ZnO hexagonal structure. The peak at 275 cm^{-1} is an additional mode caused by oxygen vacancy and impurities defects [25]. Besides, the Raman spectra of Al doped ZnO shows

another vibration mode at 578 cm^{-1}. This peak is a longitudinal optical (LO) scattering mode that resulted from higher carrier concentration [26].

3.1.3 X-ray diffraction analysis

To investigate the crystalline structure of the samples, XRD is used to confirm the structure properties and their lattice formations. Un-doped and Al doped ZnO were investigated crystalline plane by XRD in degree of 10-60°. The XRD pattern of samples is reported in Figure 3.9.

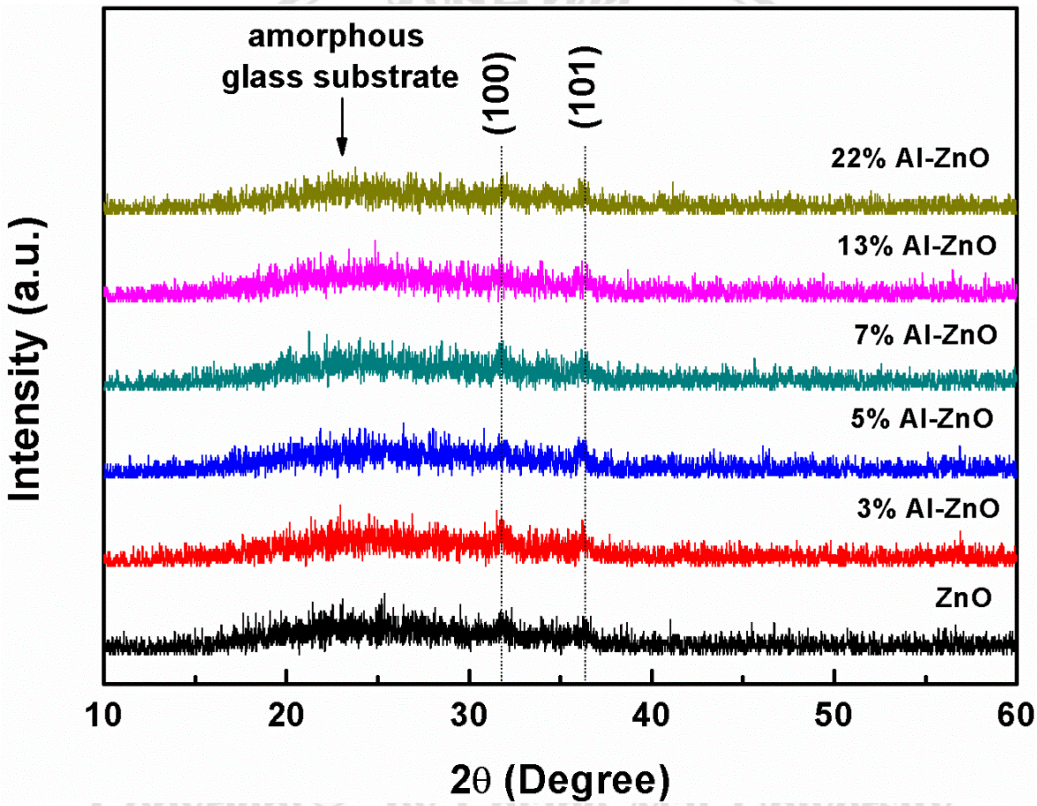

Figure 3.9 XRD pattern of un-doped and Al doped ZnO.

All samples illustrate a little peak at 31.74° and 36.22° which are correspond to the lattice planes of (100) and (101), respectively. That relates to hexagonal wurtzite ZnO phase which is similar to the reported data in Joint Committee on Powder Diffraction Standard (JCPDS), Reference code: 029272. The lattice parameters of sample are reported in Table 3.2

Table 3.2 Crystallographic parameters for ZnO.

Sample	**Un-doped and Al doped ZnO**
Crystal system	Hexagonal
a (Å)	3.253
b (Å)	3.253
c (Å)	5.213
Alpha (°)	90
Beta (°)	90
Gamma (°)	120

3.1.4 Optical property analysis

To investigate the optical properties, transmittance of both un-doped and Al doped ZnO thin films was investigated by Ultraviolet-visible spectroscopy at room temperature. The transmittance of samples was recorded in wavelength of 300-800 nm. Figure 3.10 illustrates the optical transmittance of samples.

From Figure 3.9, it is seen clearly that all samples have an average transmittance in visible region at 60 %. It is clear that the transmittance increased with increasing the doping ratio of Al. Moreover, a blue shift of the absorption edge was observed in the doped films [29]. It probably caused by the energy gap turning that resulting from Al content in ZnO.

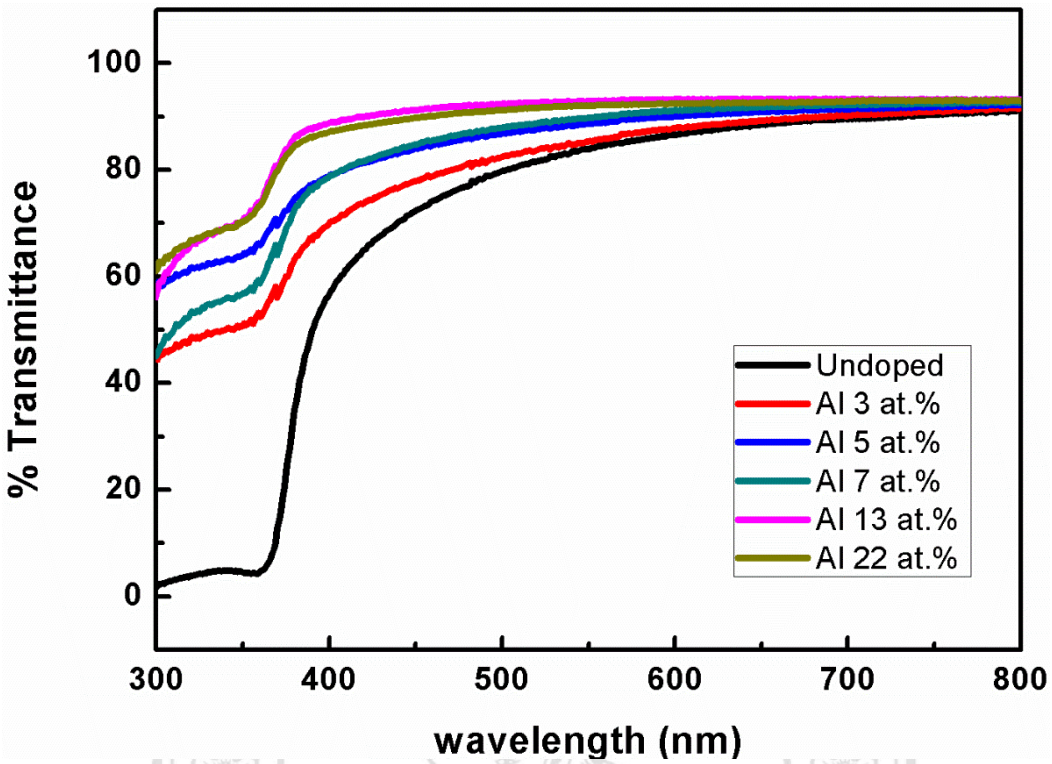

Figure 3.10 Optical transmittance of un-doped and Al doped ZnO.

To calculate the Energy gap (E_g) of the samples, it can be observed by using Tauc method which demonstrates a relationship between incident photon energy of semiconductor and absorption coefficient. The Tauc's equation is as follow [27];

$$(\alpha h\nu) = C(h\nu - E_g)^n \tag{3.2}$$

Where C is Constant

E_g is Energy gap

hν is Incident photon energy

n is equal to ½ for a direct transition semiconductor and 2 for an indirect transition semiconductor

α is Absorption coefficient, it can calculate from equation as follow;

$$\alpha = \frac{-\ln T}{d} \qquad \text{(for transmittance)} \qquad (3.3)$$

$$\alpha = \frac{2.3026A}{d} \qquad \text{(for absorbance)} \qquad (3.4)$$

Where T is Transmittance value

A is Absorbance value

d is the film thickness

For calculation the energy gap of un-doped and Al doped ZnO, n value is equal to ½ was placed to Tauc's equation. This is because typical ZnO demonstrates to the direct transition semiconductor. Equation 3.3 is used to find the absorption coefficient as follow to optical transmittance if the samples. The relation curve of $(\alpha h\nu)^2$ and $h\nu$ for each sample was plotted as shown in Figure 3.11.

Figure 3.11 shows the relation curve of $(\alpha h\nu)^2$ and $h\nu$ for each sample. The linear extrapolation for each sample was plotted, the point value of fitted linear and X axis is the energy gap (E_g) of the sample. The energy gap (E_{g1}) of the films were investigated. Moreover, the plots for Al doped ZnO films also show another energy gap (E_{g2}) that resulted from effect of Al doping. The both of energy gap value is shown in Table 3.3.

Table 3.3 Both of energy gap (E_{g1} and E_{g2}) of the AZO samples.

Sample	**Energy gap (E_{g1})**	**Energy gap (E_{g1})**
ZnO	3.34	-
3 % Al doped ZnO	3.40	3.98
5 % Al doped ZnO	3.45	4.02
7 % Al doped ZnO	3.49	4.00
13 % Al doped ZnO	3.51	4.08
22 % Al doped ZnO	3.53	3.95

The calculated energy gap (E_{g1}) was 3.34-3.53 eV. It is clearly seen that energy gap (E_{g1}) of the film increased with increasing Al doping ratio as shown in Figure 3.12. In the generally, the energy gap of ZnO is average at 3.2-3.4 eV. The Al adding to ZnO (AZO) not only had effect to shift of transmittance to higher energy, but it had effect to changing the energy gap of the doped film also. That might be result from Al content doped in. As mention in section of effect of Al doped ZnO in Chapter 1, when Al was doped into ZnO it was produce free extra electron in the conduction band of material.

Moreover, the Al doping into ZnO also illustrated an additional energy gap (E_{g2}), while un-doped ZnO film had not been E_{g2}. From calculated energy gap (E_{g2}), it was found that the E_{g2} had average energy gap of 4.00 eV. The occurrence of E_{g2} may affect from the carrier concentration in the system for AZO films which were higher than the un-doped film, furthermore the effect of impurity defect in doped film has affected to modification the energy band structure. But in this case, it is not exactly reason or principle to explain occurring the additional band of E_{g2} for the film with impurity doping.

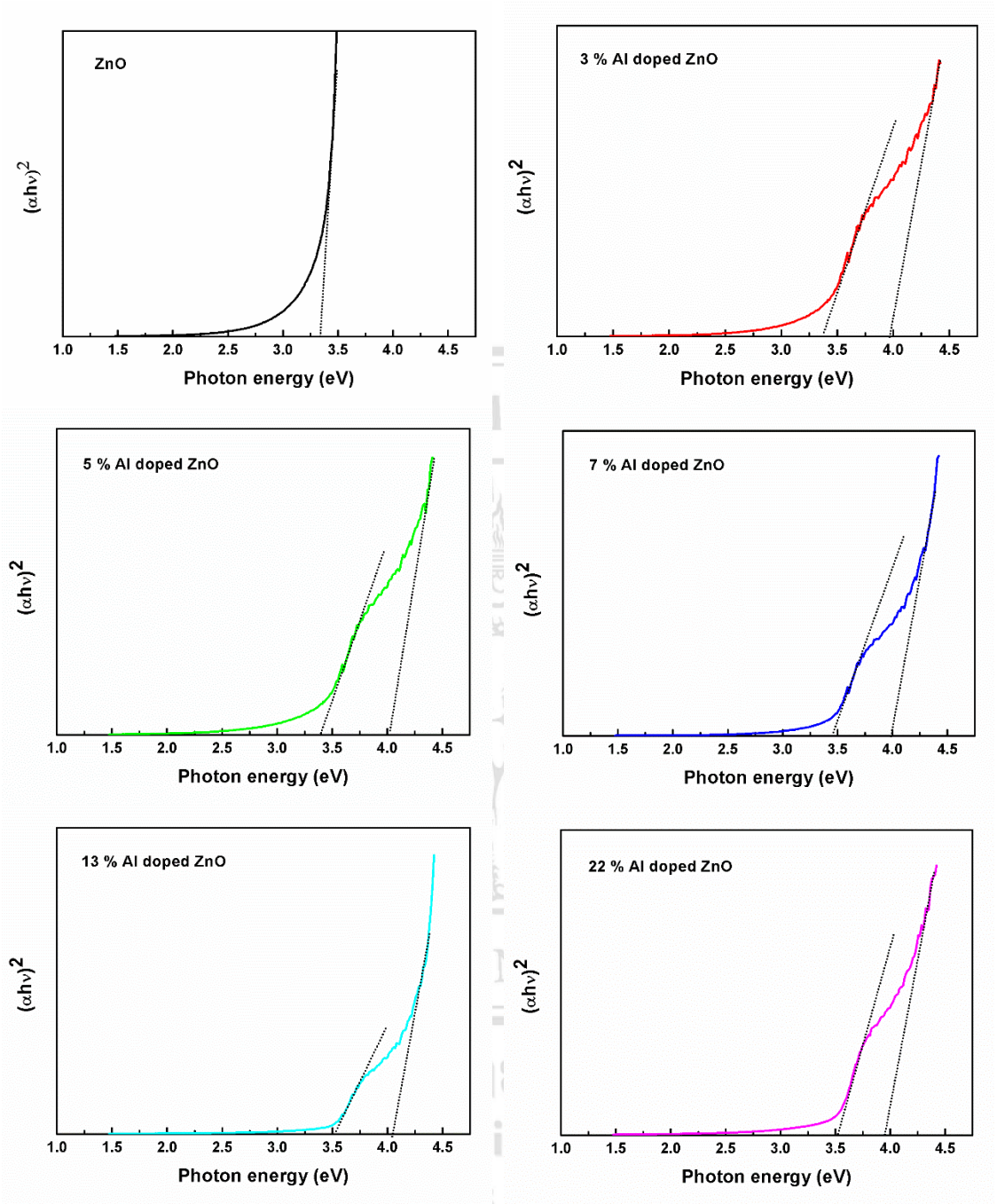

Figure 3.11 The relation curve of $(\alpha h\nu)^2$ and $h\nu$ for AZO sample.

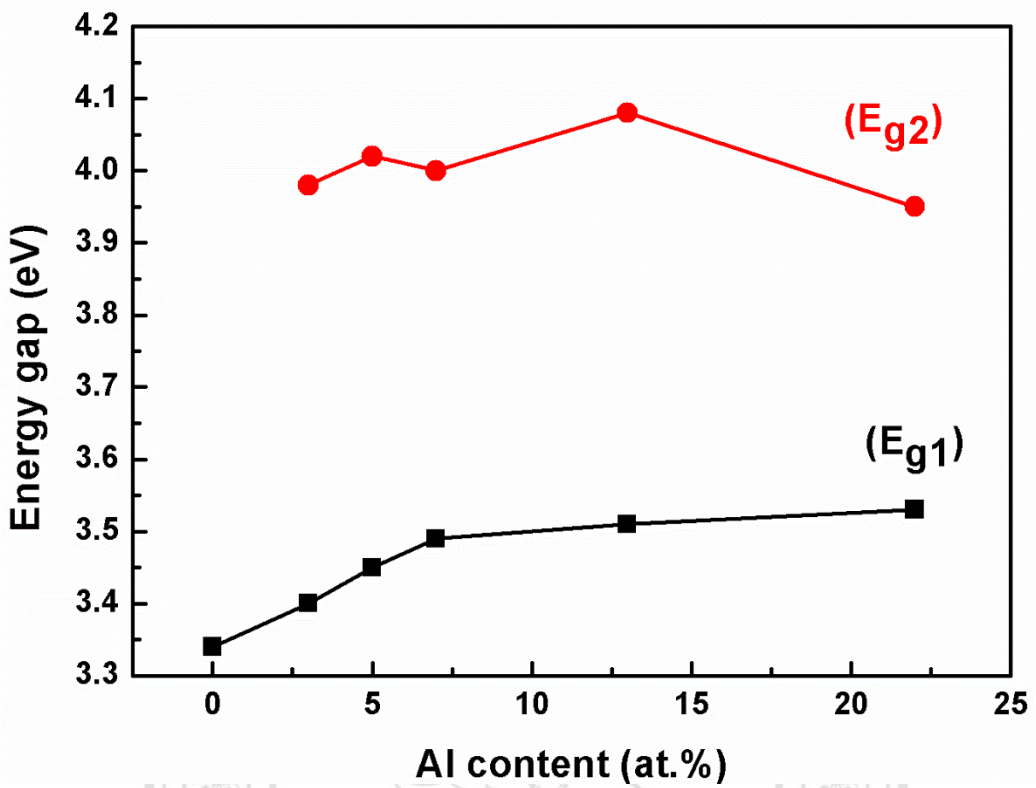

Figure 3.12 The relation of Al doping ratio in ZnO and their energy gap.

The energy gap (E_{g1}) turning can be explained by Burstein-Moss effect that is related to the electron carrier density. It can be described in the equation as follows [28]:

$$E_g = E_{g0} + \Delta E_g^{BM} = E_{g0} + \frac{h^2}{8m_e^*}\left(\frac{3}{\pi}\right)^{2/3} n_e^{2/3} \qquad (3.5)$$

where E_{g0} = The intrinsic forbidden band width

ΔE_g^{BM} = Band gap increment caused by Burstein- Moss effect

n_e = Electron carrier density

h = Planck's constant

m_e^* = effective electron mass in conduction band

Al doping into ZnO affected to increase the energy gap. It can be explained that substitution of Al^{3+} to Zn^{2+} in the AZO films, the extra e^- from Al^{3+} makes the electron carrier density increases [11], that resulted in the increasing of E_{g1} in the AZO films as illustrated in Figure 3.12.

3.1.5 Electrical property analysis

To investigate the electrical property of un-doped and Al doped ZnO, a resistivity of the samples was measured by a standard four probe technique with silver paste contact at room temperature. The resistivity was calculated form equation (2.4). The resistance of each sample is estimated by determining the slope of the fitted linear of corresponding V-I plots. The V-I curve of each sample is shown in Figure 3.13.

From Figure 3.13, the curves were fitted as a linear relation. The resistance of the samples were observed as the slope of the fitted linear. The resistivity was calculated as illustrated in Table 3.4.

Table 3.4 Resistivity of AZO films.

Sample	**Al doping ratio (atomic %)**	**Films thickness (μm)**	**Resistance [slope] (Ω)**	**Resistivity (Ω-cm)**
1	0	0.950	3.6468	7541.6249
2	3	1.136	2.8427	4910.9662
3	5	0.972	2.3594	4763.6053
4	7	1.174	3.4484	5764.5345
5	13	1.110	3.5009	6189.6720
6	22	0.956	4.0083	8228.2945

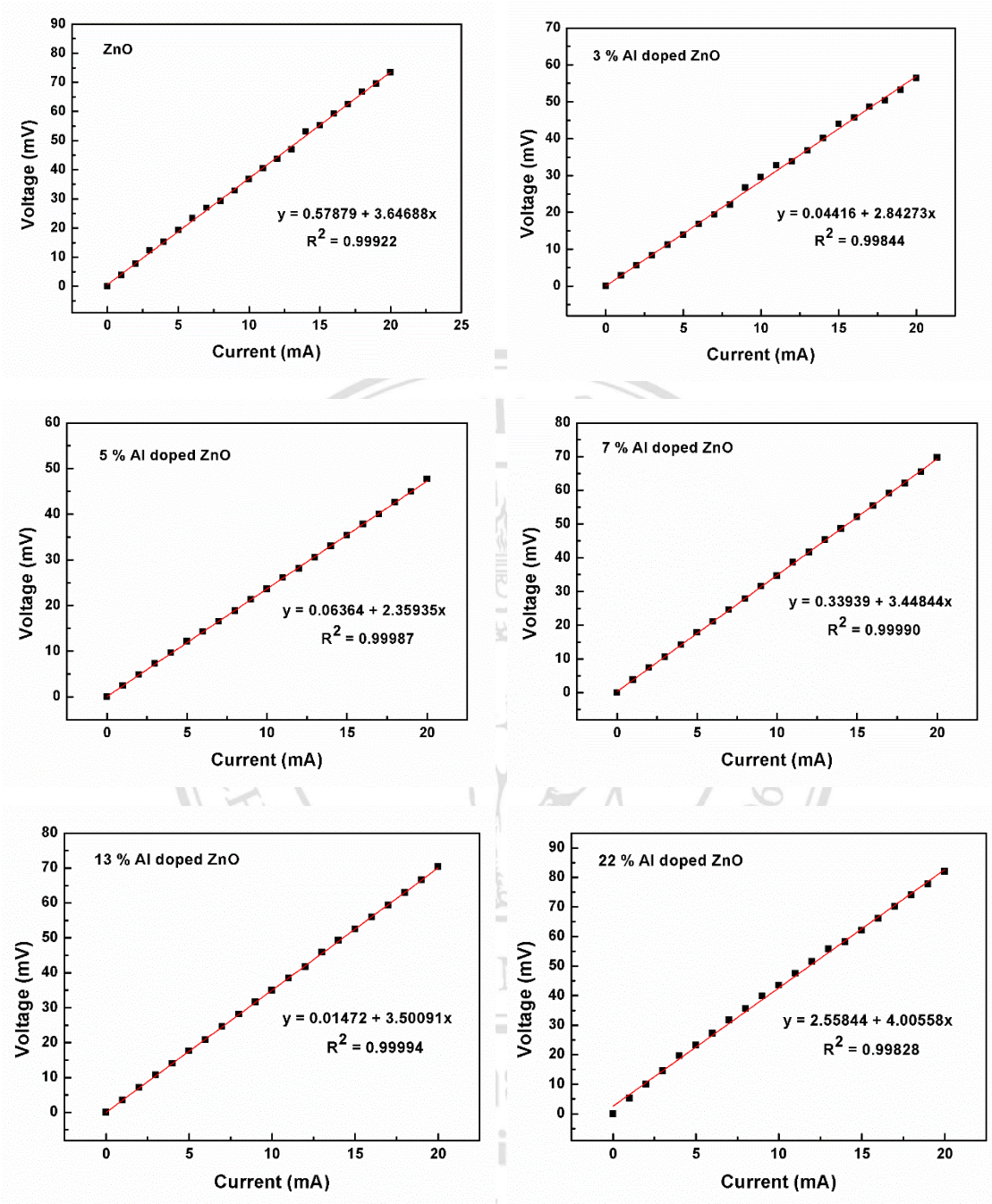

Figure 3.13 The V-I curves were fitted as a linear relation for each AZO sample.

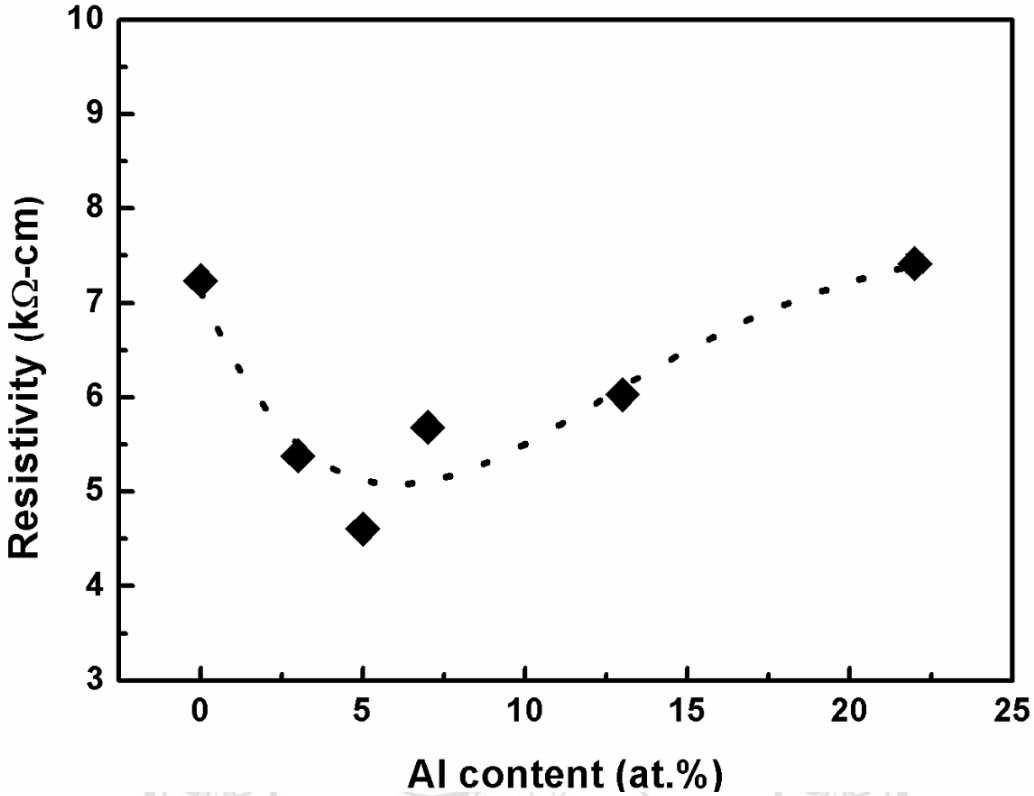

Figure 3.14 The relation graph of Al doping ratio and their resistivity.

From the resistivity result of AZO films is shown in Figure 3.14, it decreased at a small amount of Al doping as compared to the un-doped sample. As mentioned above that is about substitution of Al in ZnO, Al^{3+} provides extra free electron into the system. That make the resistivity of the film decreased. In contrast, the increase doping levels affected to increase the resistivity of doped films that may be due to an increasing of insulator Al_2O_3 concentration [29, 28]. However, the optimum of Al doping level was found at 5 at. % in AZO film for the thin film prepared by sparking process.

3.2 Cu_2O thin film

Cu_2O films were deposited on glass substrate by a sparking process under flowing argon atmosphere. The capacitance paralleled Cu tips was fixed at 40 nF. The samples were annealed at 200 °C.

3.2.1 Raman spectroscopy analysis

To examine the chemical structure, Cu_2O thin films for different annealing time were examined by Raman spectroscopy in wavelength range of 200-800 nm at room temperature using the 532 nm line of solid state laser 150 mW. The Raman spectra of the samples is shown in Figure 3.15.

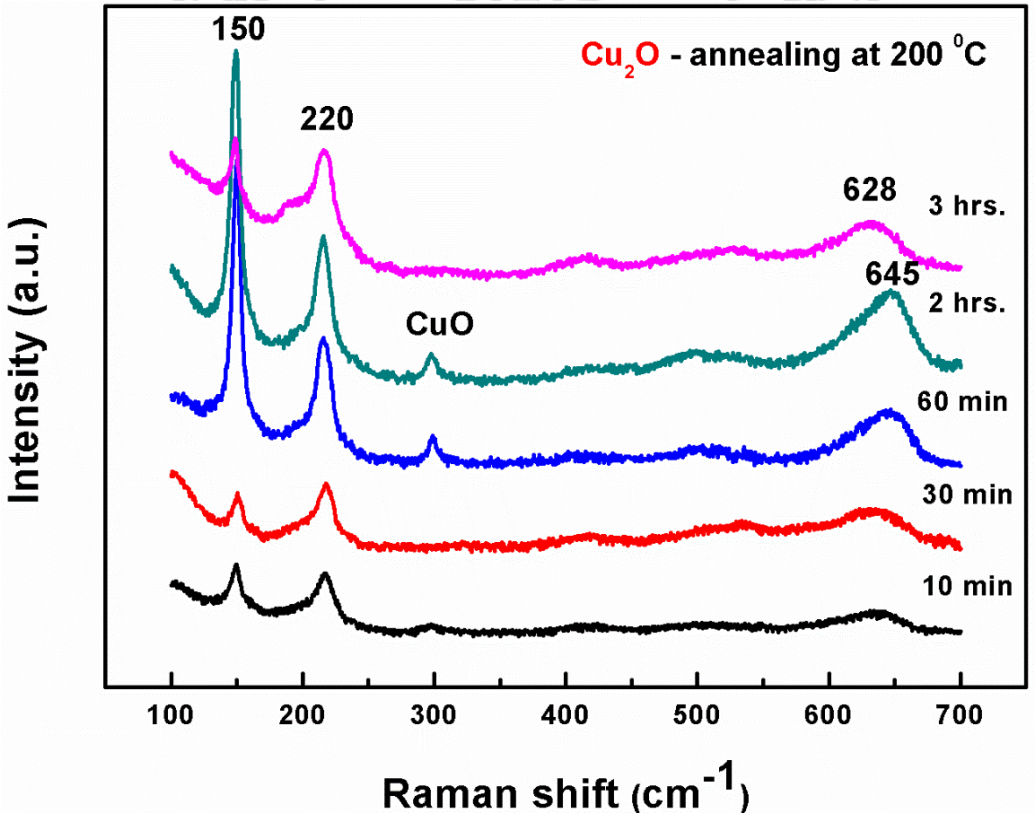

Figure 3.15 Raman spectra of Cu_2O thin film for different annealing time.

From Raman spectra of Cu_2O thin film as shown in Figure 3.15, all sample illustrate dominant peak Raman shift at 150, 220, 628, and 645 cm^{-1}. These dominant peaks are corresponded to database of Cu_2O. The peak Raman shift of 150 and 628 cm^{-1} demonstrates to IR active modes that related to a perfect Cu_2O crystal. The peak at 220

cm^{-1} is an overtone mode. In addition, the prominent peak observed for Cu_2O annealed for 60 min and 2 hrs. show a weak band at 292 cm^{-1}. This peak corresponds to CuO [30].

3.2.2 X-ray diffraction analysis

To investigate the crystalline structure of the samples, XRD is used to confirm the structure properties and their lattice formations. Cu_2O annealed at 200 °C was investigated crystalline plane by XRD in degree of 10-60°. The XRD pattern of samples is reported in Figure 3.16

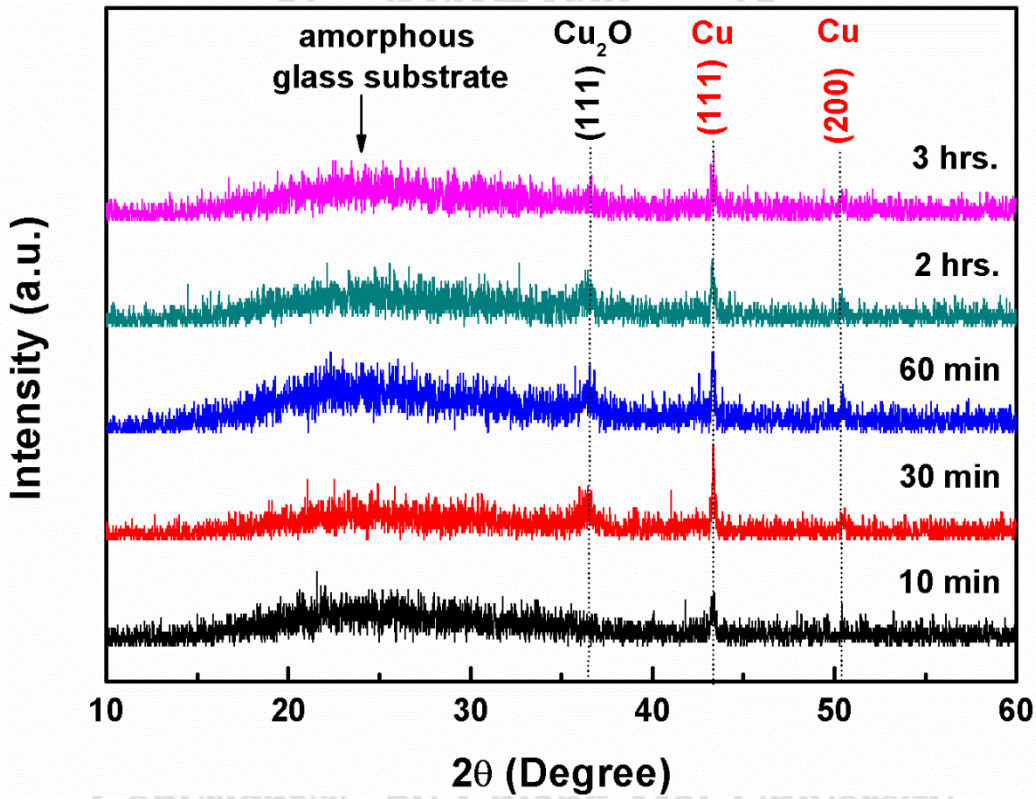

Figure 3.16 XRD pattern of Cu_2O annealed at 200 °C for different annealing time.

From XRD pattern of Cu_2O thin films as shown in Figure 3.16, all samples show a peak at 36.5° which relates to crystalline plane (111) (black color) of cubic Cu_2O. The XRD pattern of synthesized Cu_2O phase is similar to the reported data in JCPDS, Reference code: 026963, But the peak intensity of Cu_2O (111) for annealing time at 10 min is relatively low that is according to Raman spectroscopy result. Moreover, XRD pattern observed of Cu_2O thin films illustrates the peak at 43.32° and 50.45° which are

correspond to the lattice planes of (100) and (101) in red color, respectively. Both red lattice planes relate to cubic Cu phase which is similar to the reported data in JCPDS, Reference code: 064699. The lattice parameters of Cu_2O and Cu phase are reported in Table 3.5 and 3.6, respectively.

Table 3.5 Crystallographic parameters for Cu_2O.

Sample	**Cu_2O**
Crystal system	Cubic
a (Å)	4.260
b (Å)	4.260
c (Å)	4.260
Alpha (°)	90
Beta (°)	90
Gamma (°)	90

Table 3.6 Crystallographic parameters for Cu phase in Cu_2O.

Sample	**Cu phase in Cu_2O**
Crystal system	Cubic
a (Å)	3.615
b (Å)	3.615
c (Å)	3.615
Alpha (°)	90
Beta (°)	90
Gamma (°)	90

3.2.3 Optical property analysis

To investigate the optical properties, absorbance of Cu_2O thin films was investigated by Ultraviolet-visible spectroscopy at room temperature. The absorbance of samples was recorded in wavelength of 380-800 nm. Figure 3.17 illustrates the optical absorbance of sample for different annealing time.

From absorbance of Cu_2O as shown in Figure 3.17, it is clearly seen that all samples can absorb in visible region. Among these, the annealed Cu_2O at 2 hrs. shows highest absorbance up to 2 absorbance arbitrary unit in visible region.

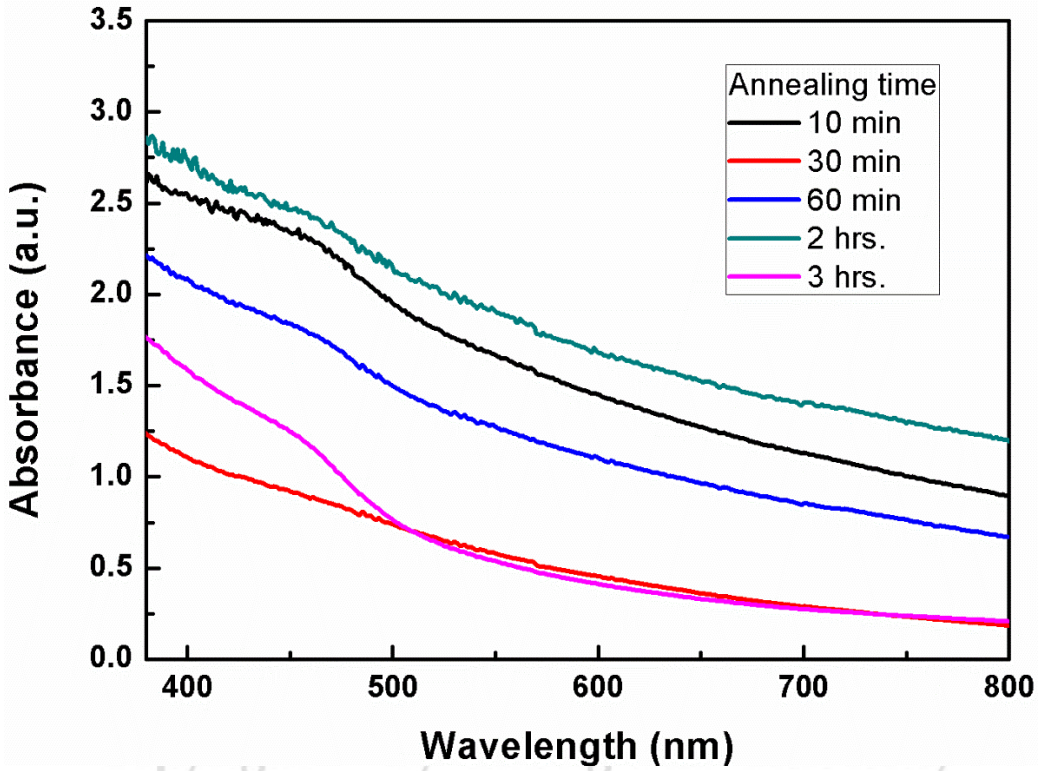

Figure 3.17 Optical absorbance of Cu_2O for different annealing time.

.

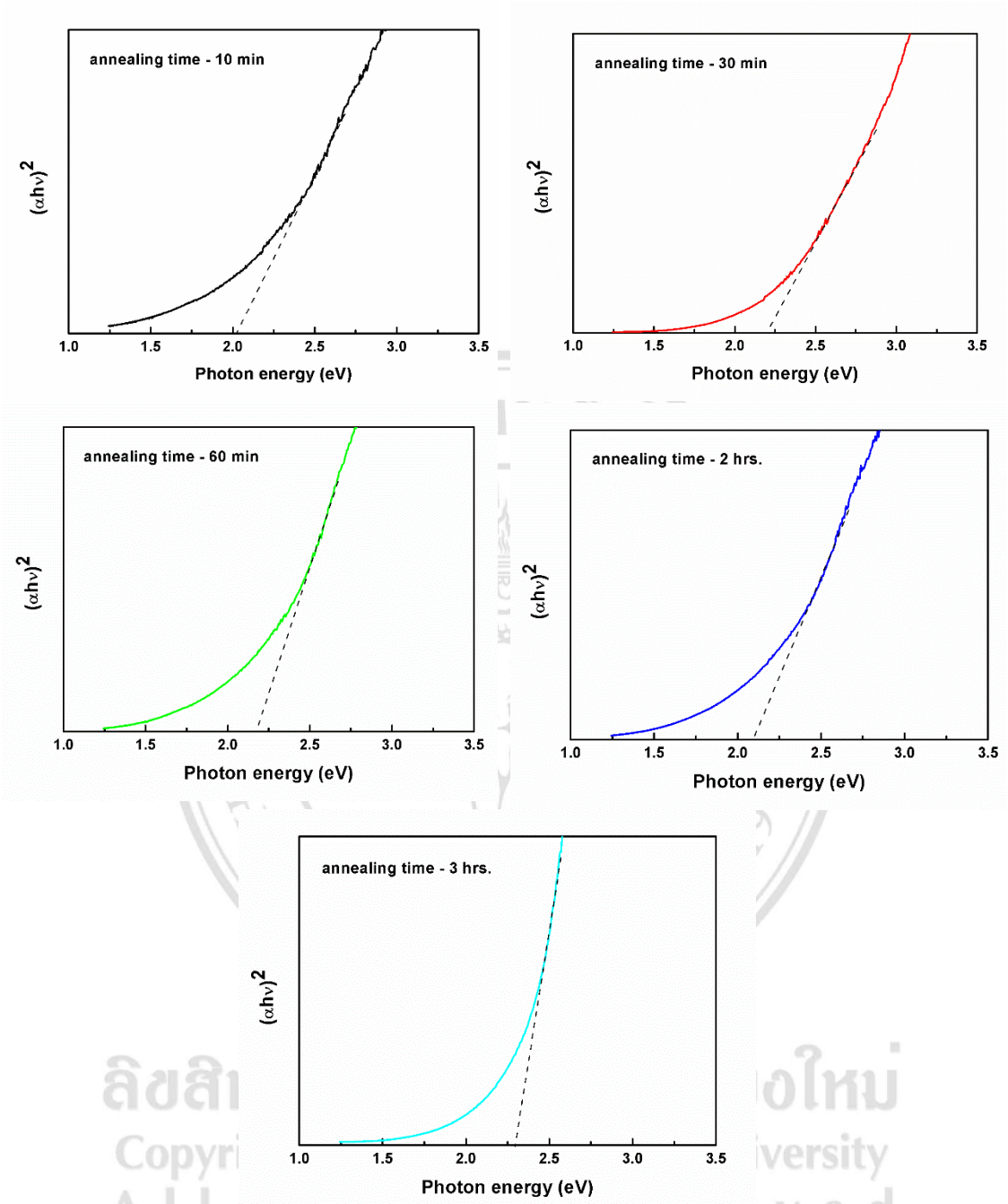

Figure 3.18 The relation curve of $(\alpha h\nu)^2$ and hν of Cu_2O for different annealing time.

To calculate the Energy gap (E_g) of the samples, it can be observed by using Tauc's equaton as follow in equation 3.2. Absorption coefficient (α) was calculated by using equation 3.4. the n value is equal to ½ was placed to Tauc's equation because typical Cu_2O is the direct transition semiconductor. The relation curve of $(\alpha h\nu)^2$ and hν for each sample was plotted as shown in Figure 3.18.

Figure 3.18 illustrates the relation curve of $(\alpha h\nu)^2$ and $h\nu$ for each sample. The linear extrapolation of Cu_2O for different annealing time was plotted, the point value of fitted linear and X axis is the energy gap (E_g) of the sample. The energy gap of the films were determined and is shown in Table 3.7.

Table 3.7 Energy gap of Cu_2O for different annealing time.

Sample	**Annealing time**	**E_g (eV)**
1	10 minutes	2.00
2	30 minutes	2.20
3	60 minutes	2.18
4	2 hours	2.10
5	3 hours	2.29

From the results of Raman spectroscopy, XRD pattern and optical property analysis, Cu_2O annealed for 2 hours demonstrates outstanding properties compared to another annealing time. Moreover, Cu_2O annealed for 2 hours illustrates the energy gap of 2.1 eV, which corresponds to typical properties of Cu_2O. Therefore, Cu_2O thin film prepared by sparking process and annealed at 200 °C for 2 hours present the highest perfect crystal of Cu_2O phase.

3.2.4 SEM image and Cross-section analysis

The surface morphology of optimize condition Cu_2O was observed by SEM at room temperature as shown in Figure 3.19. Cu_2O surface have contributed particle in regularly size all area. The particles on the top surface are bigger than the down surface, which is the effect to agglomeration of particle because of annealing treatment.

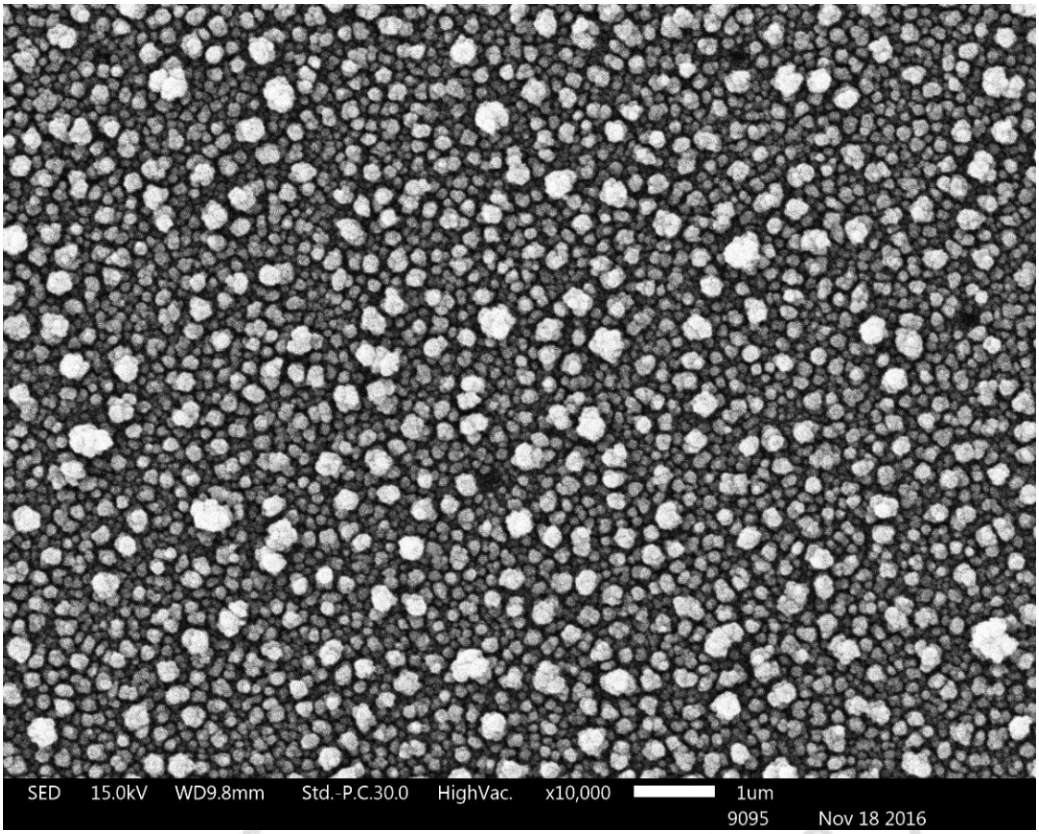

Figure 3.19 SEM surface image of Cu_2O.

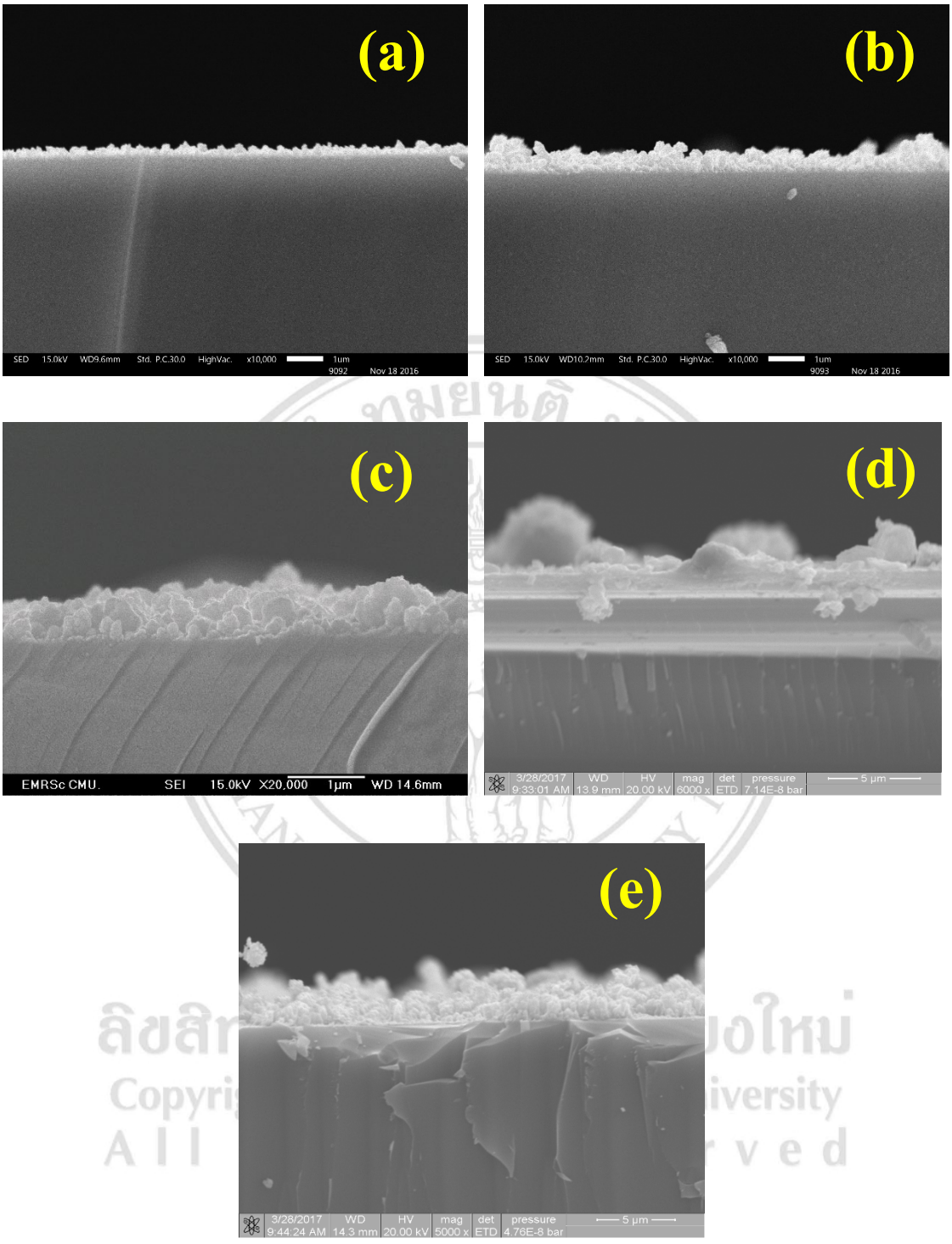

Figure 3.20 Cross-section images of Cu_2O for sparking time at (a) 20 min, (b) 40min, (c) 60 min, (d) 2 hrs., (e) 3 hrs.

From cross-section images of Cu_2O for different sparking time, a thickness of the samples were measured by an Image J program. The relation between the film thickness and sparking time of Cu_2O is plotted with a linear fitting which is shown in Figure 3.21.

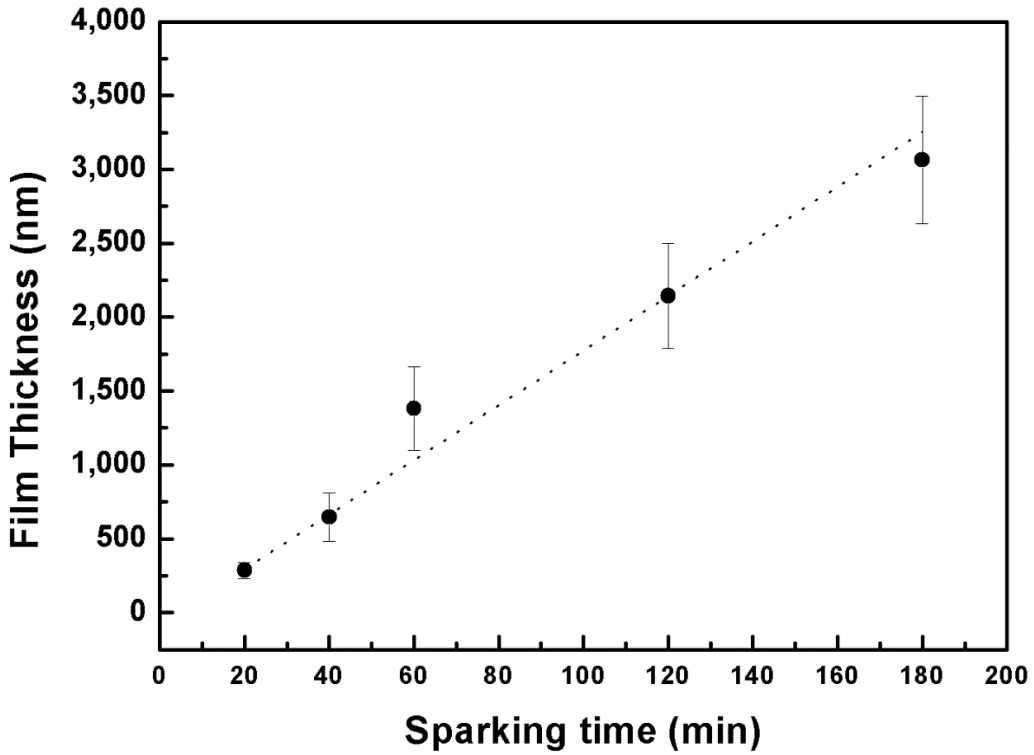

Figure 3.21 Graph relation of the film thickness and sparking time for Cu_2O.

From graph relation between the film thickness and sparking time of Cu_2O is plotted as shown in Figure 3.21, the data was fitted by linear relation. It can determine the fitted equation as follow;

$$y = -75.7938 + 18.4976x \tag{3.6}$$

From equation 3.6, we found that

Deposition rate = Slope = 18.4976 nm/min

Therefore, Cu_2O prepared by sparking process have the deposition rate at 18.4976 nm/min.

3.2.5 Electrical property analysis

To investigate the electrical property of Cu_2O, the resistivity of the samples was measured by a standard four probe technique with silver paste contact at room temperature. The resistivity was calculated form equation (2.4). The resistance of each sample is estimated by determining the slope of the fitted linear of corresponding V-I plots. The V-I curve of the sample for different sparking time is shown in Figure 3.22.

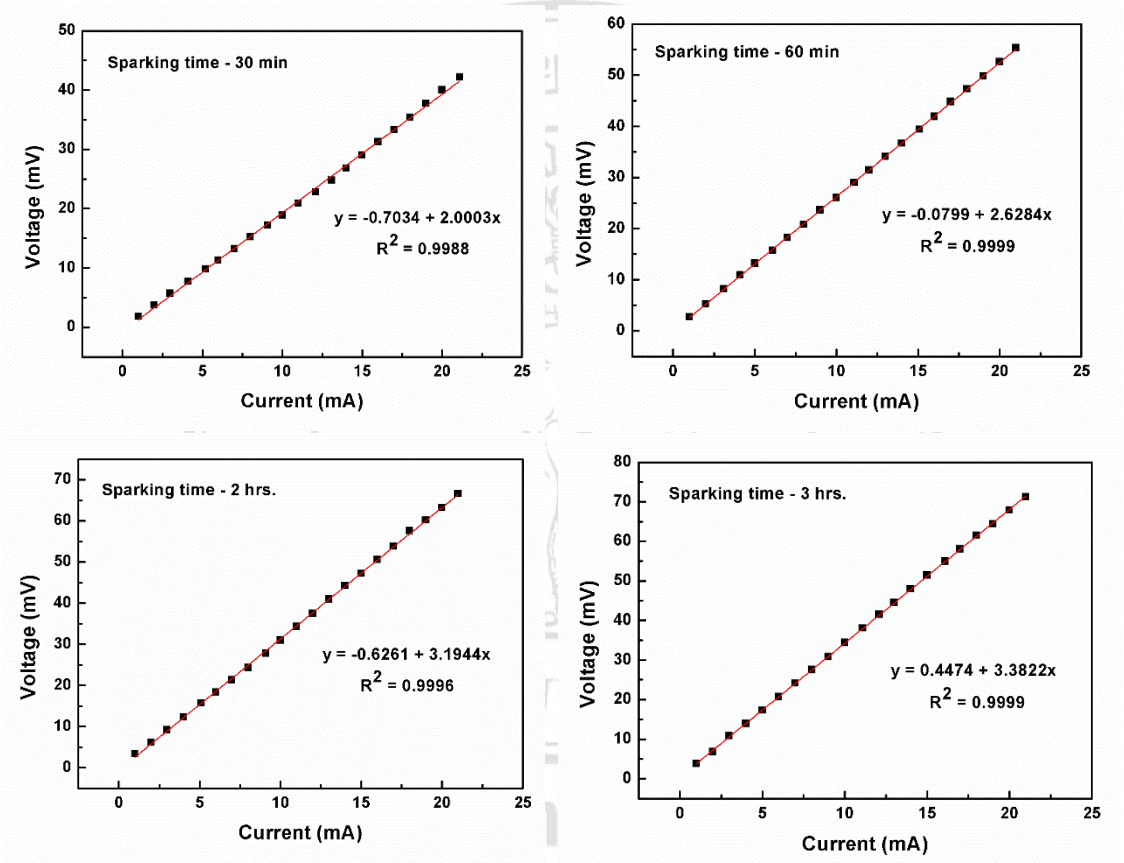

Figure 3.22 The V-I curve of Cu_2O for different sparking time.

From graph relation between the V-I curve of Cu_2O for different thickness is plotted as shown in Figure 3.22, the data was fitted by linear relation. It can determine the resistance form slope of the linear graph. The thickness of Cu_2O thin film for different sparking time can be calculated form the deposition rate of Cu_2O, as mention above. The value of resistance and the film thickness for different sparking time are shown in Table 3.8.

Table 3.8 The resistance and the thickness of Cu_2O film for different sparking time.

Sample	Sparking time	Film thickness (nm)	Resistance [slope] (Ω)
1	30 minutes	554.928	2.000
2	60 minutes	1109.856	2.628
3	2 hours	2219.712	3.194
4	3 hours	3699.520	3.382

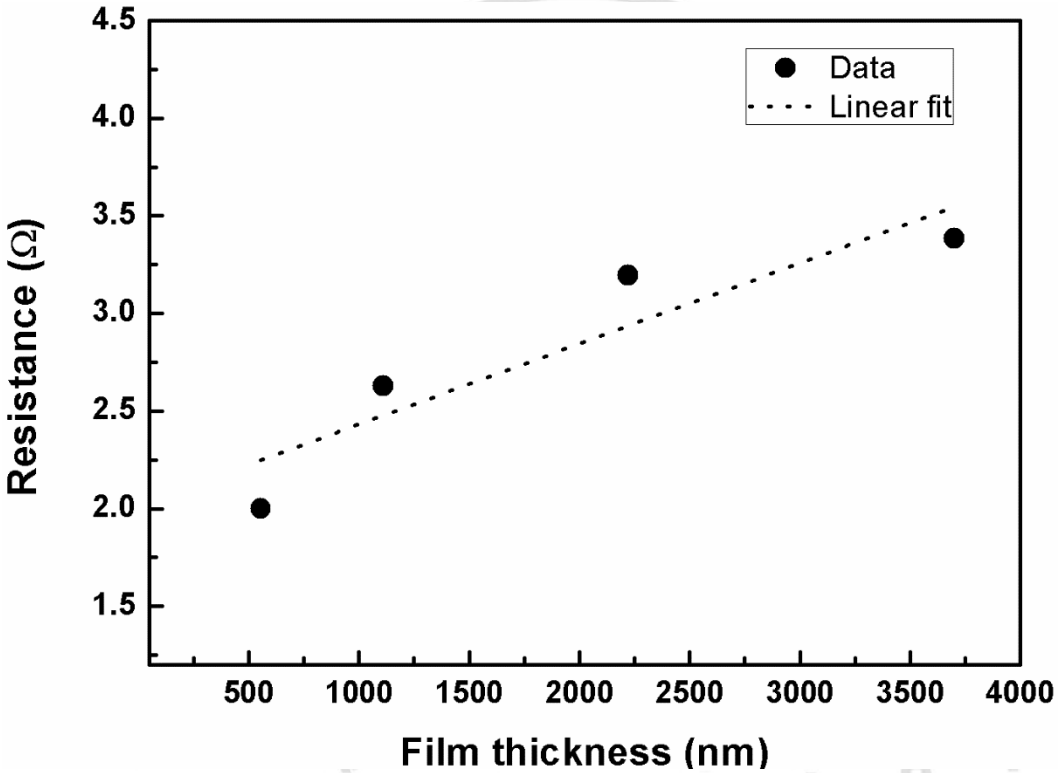

Figure 3.23 Graph relation of the film thickness and resistance and their linear fitting.

From graph relation between the film thickness and resistance of Cu_2O is plotted as shown in Figure 3.23, the data was fitted by linear relation. It can determine the fitted equation as follow;

$$y = 2.0179 + (4.1314 \times 10^{-4})x \tag{3.7}$$

From equation 3.7, we found that

Resistance/length = Slope = 4.1314×10^{-4} Ω/nm

According to equation (2.4), the effective area of the measuring electrode (A) for the sample was equal to 0.19625 cm^2 (a circle area with a radius of 0.25 cm.). The resistivity (ρ) of Cu_2O thin film can be determined by

$$\rho = \left(\frac{R}{L}\right)A = (4.1314 \times 10^{-4}\ \frac{\Omega}{nm}) \bullet (0.19625 cm^2)$$

And then,

$$\rho = 810.7873\ \Omega.cm$$

Therefore, the resistivity of Cu_2O film prepared by sparking process is equal to 810.7873 Ω.cm

3.3 AZO/Cu_2O Heterojunction

AZO/Cu_2O Heterojunction was fabricated by the sparking process. The first layer of AZO thin film was deposited on a Fluorine doped Tin Oxide (FTO) substrate and was annealed at 400 °C for 60 min. The Cu_2O layer was deposited on AZO as a second layer and was annealed at 200 °C for 2 hrs. The two step sparking process were done under flowing Ar atmosphere with a flow rate of 0.5 L/min at room temperature. A silver paste contact was used as an electrode.

3.3.1 SEM Cross-section image

From cross-section image of AZO/Cu_2O heterojunction, It can be seen clearly that AZO and Cu_2O were separated as two junction. The first level below was AZO thin film and the second level was Cu_2O. The morphology of Cu_2O from cross-section view shows a porous of agglomerated Cu_2O particles.

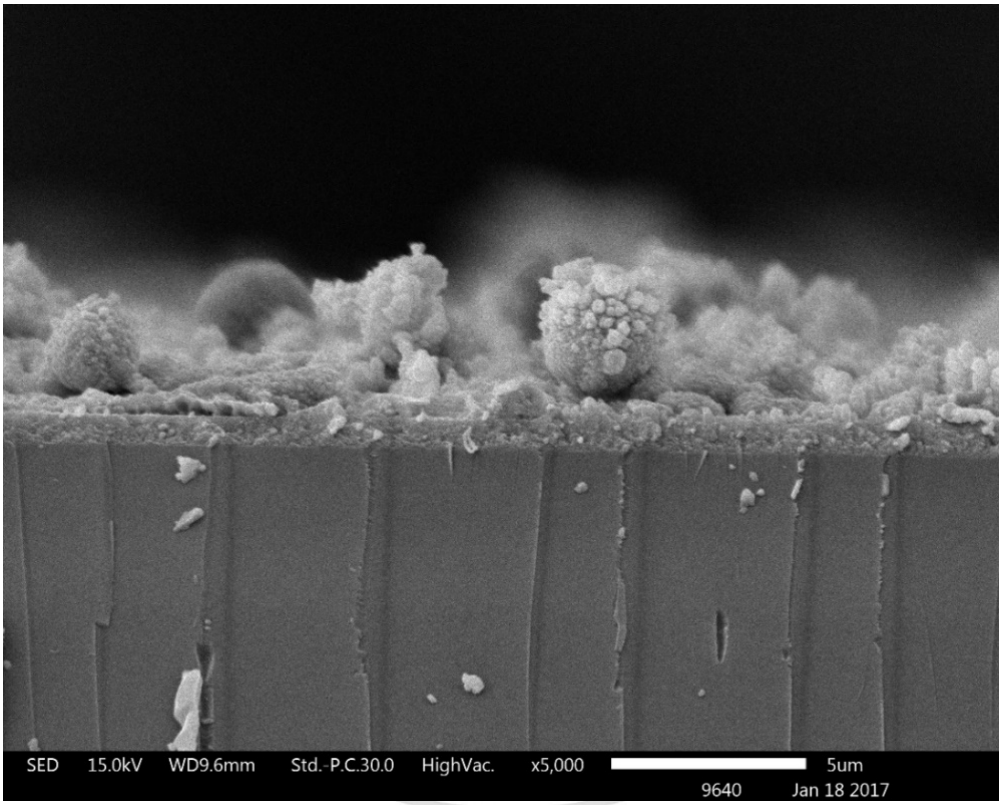

Figure 3.24 Cross-section image of AZO/Cu_2O heterojunction.

3.3.2 X-ray diffraction analysis

To investigate the crystalline structure of AZO/Cu_2O heterojunction, XRD is used to confirm the structure properties and their lattice formations. The sample was investigated crystalline plane by XRD in degree of 10-60°. The XRD pattern of sample is reported in Figure 3.25

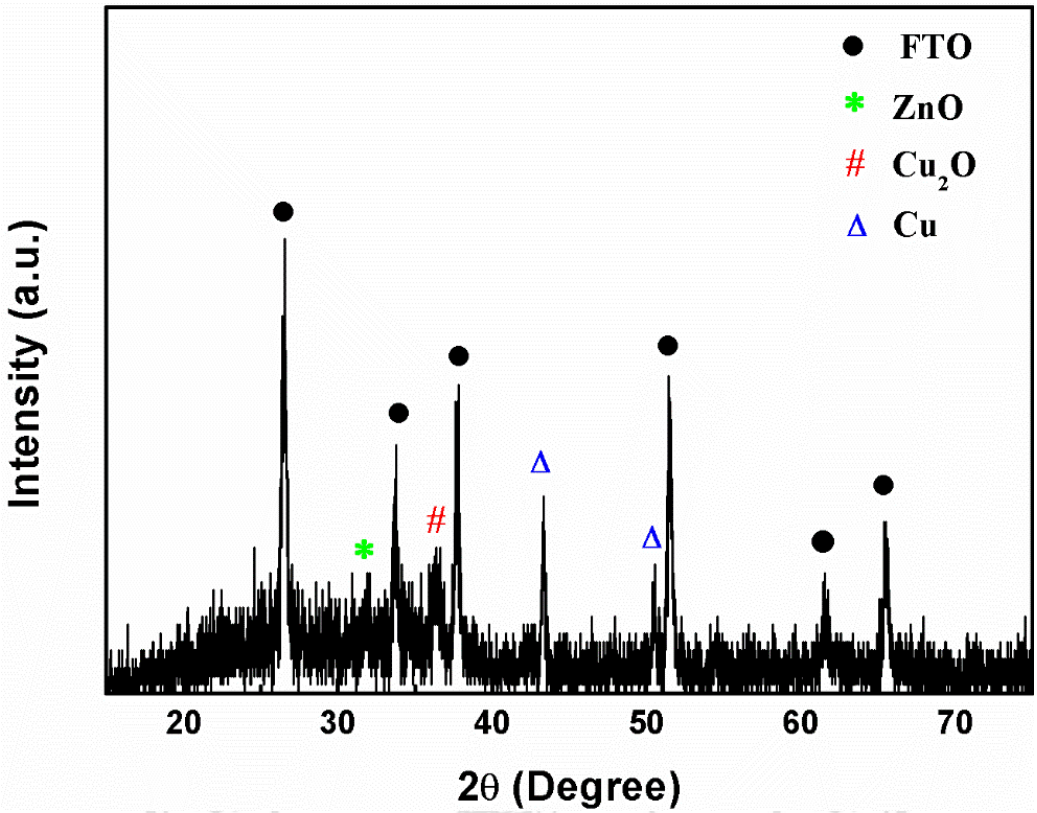

Figure 3.25 XRD pattern of AZO/Cu_2O heterojunction prepared on a FTO substrate.

From experiment part of fabrication of AZO/Cu_2O heterojunction, the heterojunction was fabricated on FTO substrate by two step sparking process. The XRD pattern illustrates XRD peaks of ZnO, Cu_2O and FTO substrate. In addition, it also shows XRD peaks of Cu which is a phase in Cu_2O.

3.3.3 Optical property analysis

To investigate the optical properties, absorbance of AZO, ZnO and Cu_2O thin films was investigated by Ultraviolet-visible spectroscopy at room temperature. The absorbance of samples was recorded in wavelength of 380-800 nm.

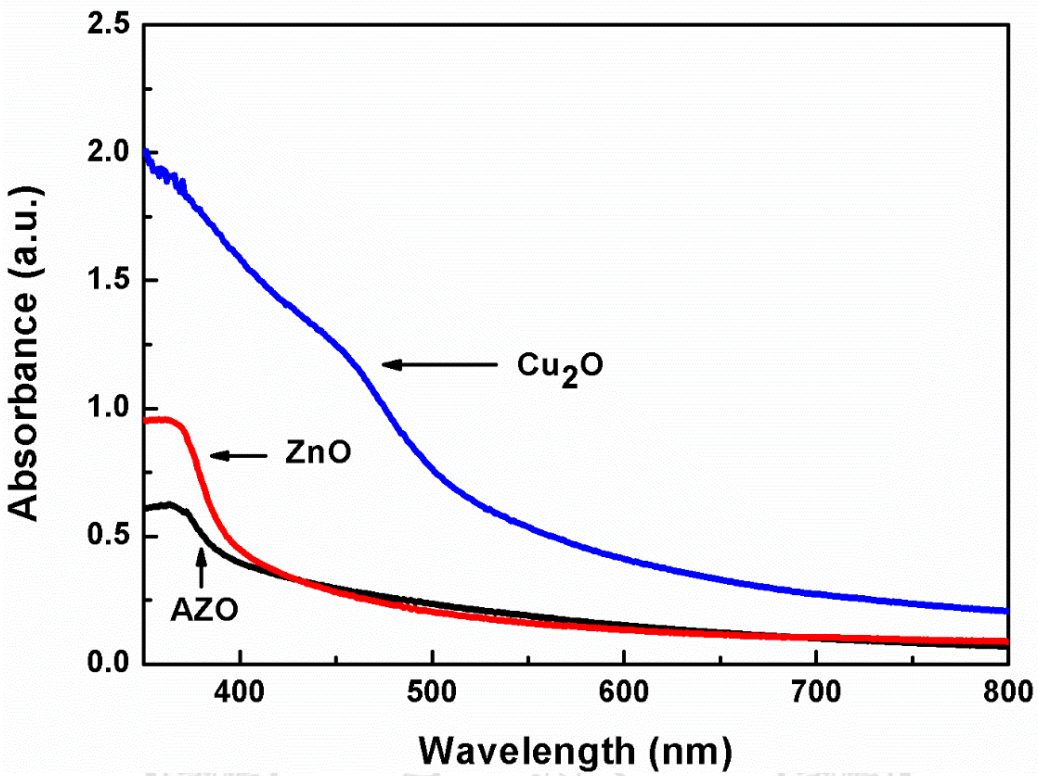

Figure 3.26 Absorbance of AZO, ZnO and Cu_2O thin films.

From absorbance of AZO, ZnO, Cu_2O thin films as shown in Figure 3.26, AZO and ZnO have been absorbance in wavelength lower than 400 nm (Ultraviolet region), which is correspond to their energy gap of 3.0-3.2 eV. On the other hand, Cu_2O has been absorbance in visible and ultraviolet regions (wavelength lower than 600 nm) because its energy gap is 2.1 eV.

The AZO/Cu_2O heterojunction can be innovated to be a p-n junction solar cell. Cu_2O is a p-type semiconductor and used as an absorption layer. From its energy gap of 2.1 eV, Cu_2O can absorb photons in visible region and generate electron-hole pairs. AZO is an n-type semiconductor and used as electron acceptor layer. It accepts electron from Cu_2O.

3.3.4 Current-Voltage (I-V) Characteristic

P-n junction are formed by joining a-type and n-type semiconductor. The n-type region has electrons are majority carrier concentration and the p-type has holes are majority carrier concentration. Current-Voltage curve has been used to study a p-n junction characteristic and transportation mechanisms of the carrier between the junctions. The n-type AZO/p-type Cu_2O heterojunction with silver paste contact was forward bias voltage condition in dark by using triangle signal generator. The current (dark current) was measured by using a multimeter at room temperature. The I-V curve of AZO/Cu_2O heterojunction is shown in Figure 3.27.

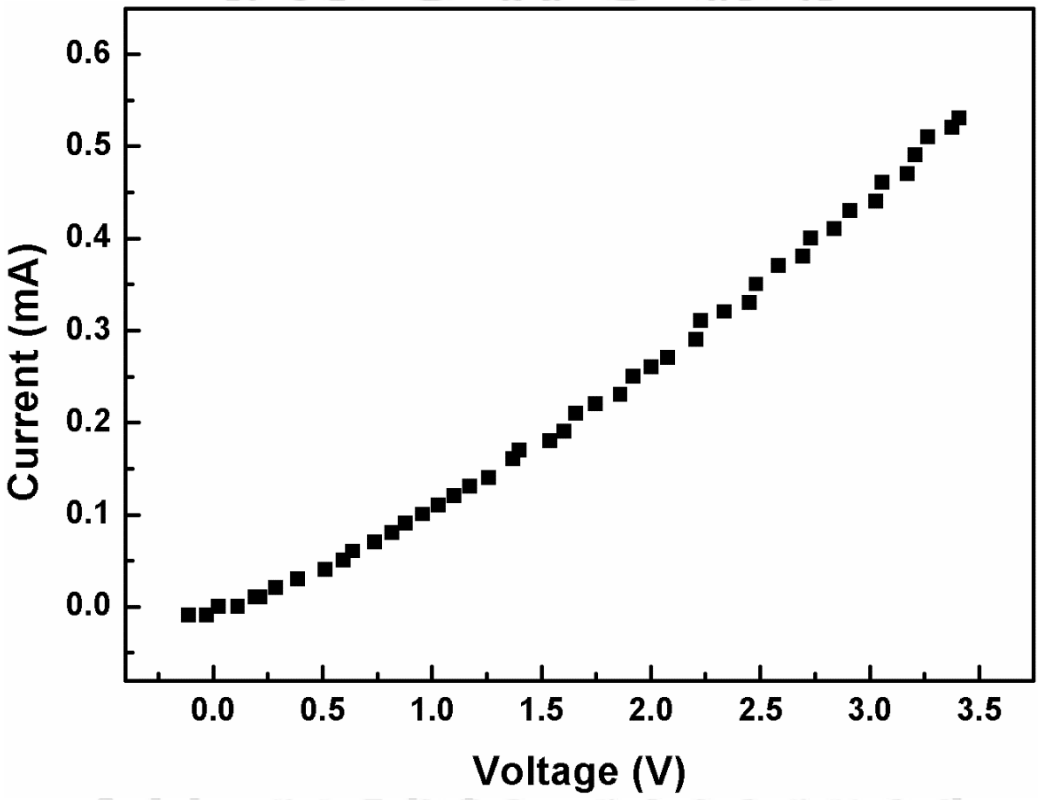

Figure 3.27 I-V curve of n-type AZO/p-type Cu_2O heterojunction.

The study of a dark forward I-V curve demonstrated the probable transportation mechanisms of the carrier between the junctions via the ideality factor (n). In generally, the ideality factor has been used to explain carrier transportation mechanisms, which includes diffusion process, carrier recombination process and tunneling process, in the presence of the electrified in the depletion region.

Moreover, the ideality factor can be studied from the dark current behavior that is results from I-V characteristic. The Diode equation is used to explain the dark current behavior, which could be described as follows;

$$J = J_0\left[\exp\left(\frac{qV}{nkT}\right)-1\right] \tag{3.8}$$

where J = The net current flowing though the diode in any area

J_0 = Dark saturation current in any area

V = Applied voltage across the terminals of the diode

q = Absolute value of electron charge

k = Boltzmann's constant

T = Absolute temperature (K)

From equation (3.9), the ideality factor (n) value was computed from the slope of the linear part in the forward ln(I)-V curve though the following relationship;

$$n = \frac{q}{kT}\left(\frac{V}{\ln J}\right) = \frac{q}{kT}\frac{1}{slope} \tag{3.9}$$

Fundamentally, the explanation of n value is,

n = 1 the predominant transportation mechanisms of the carrier is a diffusion process.

1< n <2 the predominant transportation mechanisms is a carrier recombination process.

n > 2 the predominant transportation mechanisms of the carrier is a tunneling process.

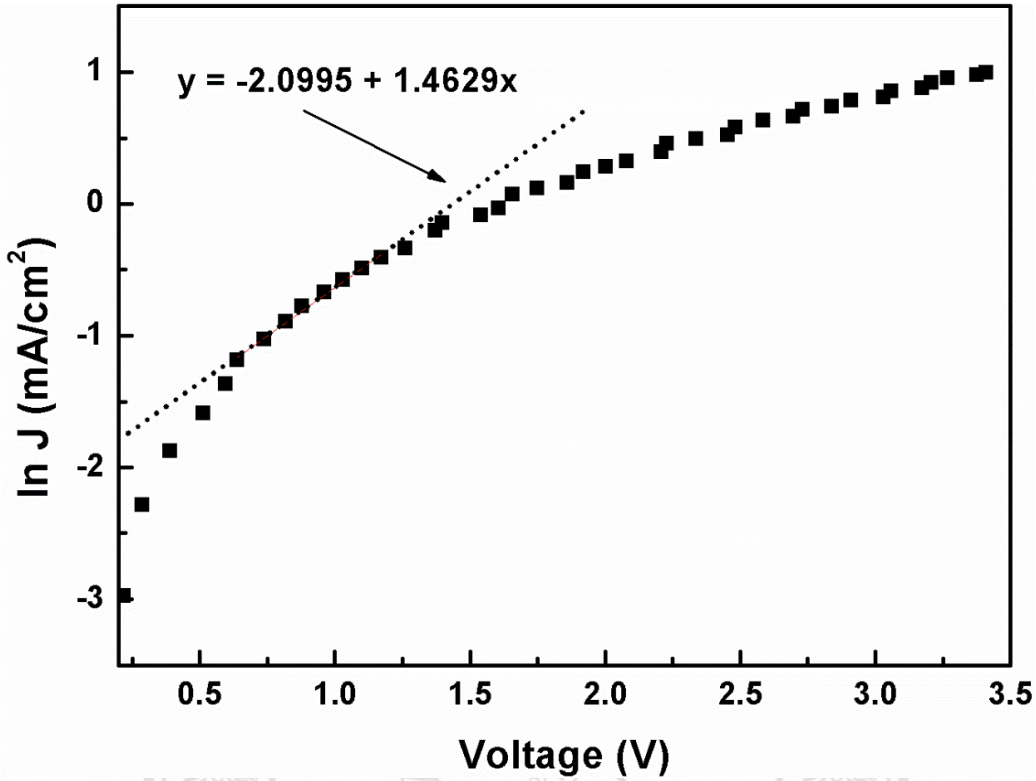

Figure 3.28 ln (I)-V curve of n-type AZO/p-type Cu_2O heterojunction with fitted linear part.

From the graph as shown in Figure 3.28, the linear was fitted at the voltage was lower than 1.15 V. The slope was determined from the linear equation. From the computation using equation (3.9), the n value was 2.644. The implication is the predominant transportation mechanism at the heterojunction interface between the n-type AZO/p-type Cu_2O was the tunneling process.

According to the cross-section image of AZO/Cu_2O heterojunction as shown in Figure 3.24, it can see that there are small gap in heterojunction interface that affected from the Cu_2O film structure had porous of agglomerated particles. Therefore, the mechanism of electron transportation form p-type Cu_2O to n-type AZO was the tunneling process in depletion region.